

Targeted Hydrogen Decrepitation of NdFeB Magnets from Large

Commercial Assemblies



UNIVERSITY OF
BIRMINGHAM

Jonathan Meakin

Student ID number: 0871064

MRes Thesis

Supervisors: Dr Allan Walton & Dr Andrew Williams

Magnetic Materials Group, Metallurgy and Materials

UNIVERSITY OF
BIRMINGHAM

University of Birmingham Research Archive

e-theses repository

This unpublished thesis/dissertation is copyright of the author and/or third parties. The intellectual property rights of the author or third parties in respect of this work are as defined by The Copyright Designs and Patents Act 1988 or as modified by any successor legislation.

Any use made of information contained in this thesis/dissertation must be in accordance with that legislation and must be properly acknowledged. Further distribution or reproduction in any format is prohibited without the permission of the copyright holder.

Synopsis

Nd-Fe-B magnets are used in a number of important applications, such as generators in gearless wind turbines, and in electric motors for vehicles and computer hard drives. In recent years there has been a big drive towards recycling of NdFeB magnets due to supply constraints for rare earth metals. Workers at the University of Birmingham have previously shown that hydrogen can be used as a processing gas to reduce NdFeB magnets to a soft magnetic hydrided powder which can be removed from electronic components (using the hydrogen decrepitation process – HD) [Walton et al, 2012]. The extracted material can be used to re-manufacture new NdFeB magnets directly from the alloy powders. The work outlined in this project has focused on the use of hydrogen to remove individual or all sintered NdFeB magnets from large commercial rotor assemblies, with the aim of re-using the underlying structure once the magnets are removed. Masking agents were successfully used to protect some regions on commercial assemblies during hydrogen decrepitation which resulted in targeted removal of specific magnets. The thermal and mechanical impact of the hydrogen decrepitation process was assessed during hydrogen processing. For all forms of sintered NdFeB scrap the surface condition of the magnets is important as oxidation has been shown to inhibit the onset of the hydrogen decrepitation process. In this work a systematic study has been performed on the early stages of oxidation in atmospheric conditions using raman spectroscopy, scanning electron microscopy and 3-D laser confocal microscopy. The oxidation behaviour has been shown to be quite different from previous studies on bulk sintered magnets at higher temperatures [Edgley, 1997] with grain boundary oxidation dominating in this lower temperature regime. It is evident that to guarantee that the hydrogen decrepitation process will be successful some surface damage will be required to break up the oxide prior to hydrogen processing. In this work the surface damage was created by scoring the surface of the magnets with a scalpel. In the final part of this project the impact of encapsulation on NdFeB magnets was investigated during the HD process by sleeving sintered NdFeB magnets in copper.

Acknowledgements

I would like to thank the EPSRC for providing funding for this work and The School of Metallurgy and Materials for providing equipment, facilities and support during the project. I would especially like to thank Dr. Allan Walton for his supervision which included putting a roof over my head when I most needed it. I would also like to thank the rest of the Magnets Materials Group and Hydrogen Group at the University of Birmingham for their support and friendship throughout. This project is dedicated to Dr. Andrew Williams who sadly passed away during the course of the project.

Table of Contents

| | |
|---|-----------|
| List of Tables | x |
| Nomenclature | xi |
| 1. Introduction | 1 |
| 2. Literature Survey | 5 |
| 2.1. Properties of Permanent Magnetic Materials | 8 |
| 2.2.1. <i>Paramagnetism</i> | 9 |
| 2.2.2. <i>Diamagnetism</i> | 10 |
| 2.2.3. <i>Ferromagnetism</i> | 10 |
| 2.2.4. <i>Ferrimagnetism</i> | 11 |
| 2.2.5. <i>Anti-ferromagnetism</i> | 11 |
| 2.3. Magnetocrystalline Anisotropy | 11 |
| 2.4. Magnetic Hysteresis | 14 |
| 2.5. Coercivity mechanisms | 16 |
| 2.6. NdFeB | 17 |
| 2.6.1. $Nd_2Fe_{14}B$ | 17 |
| 2.6.2. $Nd_{1+\epsilon}Fe_4B_4$ | 18 |
| 2.6.3. <i>Nd-rich phase</i> | 19 |
| 2.7. Processing of NdFeB magnets | 19 |
| 2.7.1. <i>Resin Bonded Magnets</i> | 19 |
| 2.7.2. <i>Sintered NdFeB magnets</i> | 20 |
| 2.8. Oxidation and corrosion of NdFeB magnets | 22 |
| 2.8.1. <i>Surface finish</i> | 23 |
| 2.9. Additions to NdFeB | 24 |
| 2.9.1. <i>Dysprosium</i> | 24 |

| | |
|---|-----------|
| 2.9.2. Cobalt | 27 |
| 2.9.3. Copper | 27 |
| 2.9.4. Aluminium | 27 |
| 2.9.5. Niobium | 28 |
| 2.10. Recycling of NdFeB | 29 |
| 3. Aims | 33 |
| 4. Experimental Procedure | 34 |
| 4.1. Starting materials | 34 |
| 4.2. Hydrogen Processing | 34 |
| 4.3. Coating Experiments | 34 |
| 4.4. Commercial Assembly Experiments | 34 |
| 4.5. Flat Plate Assembly | 35 |
| 4.6. MagScan | 36 |
| 4.7. Microscopy | 36 |
| 4.8. Raman Spectroscopy | 37 |
| 4.9. Encapsulation Experiments | 38 |
| 5. Results and Discussion | 39 |
| 5.1. Selective Removal of NdFeB Magnets | 39 |
| 5.1.1. Coating Experiments | 39 |
| 5.2. Commercial Assemblies | 41 |
| 5.3. Oxidation Experiments | 44 |
| 5.3.1. SEM imaging | 44 |
| 5.3.2. SEM with EDS | 45 |
| 5.3.3. SEM with WDS | 47 |
| 5.3.4. Confocal Microscope Observations of Oxide Growth Morphology and Kinetics | 49 |
| 5.3.5. Raman Spectroscopy | 54 |

| | |
|--|-----------|
| 5.4. Scoring experiments..... | 58 |
| 5.4.1. 3D confocal Microscopy | 58 |
| 5.5.1. Flat Plate Assembly | 61 |
| 5.5.2. MagScan..... | 66 |
| 5.6. Encapsulation of NdFeB magnets | 68 |
| Where: F is the force extended circumferentially on the cylinder wall; t is the radial thickness of the cylinder; l is the axial length of the cylinder. Therefore, equation 7 was used in order to provide a rough estimate of the forces developed during hydrogen decrepitation. | 71 |
| 6. Conclusions | 71 |
| 7. References..... | 76 |

List of Figures

| | |
|---|----|
| Figure 1 – World total installed capacity of wind turbines in MW. Gutfleisch, 2011. | 1 |
| Figure 2 - Percentage of wind energy produced by countries worldwide. Gutfleisch, 2011..... | 2 |
| Figure 3 - A history of permanent magnet development in the 20th Century - http://www.magnets.bham.ac.uk/magneticmaterials/historupdatey.shtml <viewed on the 29/06/2011> | 6 |
| Figure 4 - A periodic table showing the elements that are ferromagnetic, paramagnetic, antiferromagnetic and diamagnetic. Zakotnik 2004..... | 12 |
| Figure 5 - Hysteresis Loop for a ferromagnetic material. | 15 |
| Figure 6 – SEM image of sintered NdFeB. Zakotnik (2009)..... | 17 |
| Figure 7 - Crystal Structure of Nd ₂ Fe ₁₄ b – (Herbst, 1985)..... | 18 |
| Figure 8 - Production of rare-earth magnets via sintering..... | 20 |
| Figure 9 – The effect of dysprosium content on the remanence and coercivity of NdFeB magnets and the typical applications of these materials..... | 25 |
| Figure 10 - The effect of Dy content on the magnetic properties of NdFeB. It can be observed that there is an improvement in coercivity, a reduction in remanence and an increase in BH _{max} up to 1 wt % Dy content. (Yu, 2004)..... | 26 |
| Figure 11 -Effect of Nb content on the magnetic properties of NdFeB. It can be observed that there is an increase in coercivity, an increase in BH _{max} with up to 1 wt % Nb content and a slight reduction in remanence. (Yu, 2004)..... | 28 |
| Figure 12 - Schematic of hydrogen decrepitation..... | 30 |
| Figure 13 – Production and recycling route for NdFeB voice coil magnets for hard disk drives. Walton et al [2012]. | 32 |
| Figure 14 - Schematic diagram of the commercial rotor assembly from a Smart car. Each individual magnet was approximately 1cm x 4cm..... | 35 |

| | |
|--|----|
| Figure 15 - Mock Flat plate assembly before hydrogen exposure with temperature sensors attached. | 36 |
| Figure 16 – Schematic diagram of the NdFeB magnet encapsulated in a Cu ring. | 38 |
| Figure 17 - Voice coil magnets coated in a) Nail Varnish b) Lithographic Correction Fluid c) TEOS d) uncoated. | 40 |
| Figure 18 - Photographs of the commercial assembly a) before b) Half the magnets were scored and half were left un-scored c) after hydrogen decrepitation | 43 |
| Figure 19 - Backscattered SEM image of NdFeB magnet..... | 44 |
| Figure 20 - Backscattered SEM image of NdFeB magnet with a composition of Nd _{12.52} Pr _{0.17} Dy _{1.8} Fe _{72.49} B _{6.44} Al _{0.88} Co _{4.98} Nb _{0.61} at%, which had been exposed to air for over 1 year. | 45 |
| Figure 21 - EDS spectrum for the Nd rich phase in NdFeB magnet displaying that the spot mainly consisted of neodymium..... | 46 |
| Figure 22 - EDS spectrum for matrix phase of NdFeB magnet displaying that the spot over the matrix phase consisted of mainly iron with a smaller amount of neodymium..... | 47 |
| Figure 23 - W.D.S and E.D.S line scan of the oxygen content in an NdFeB magnet..... | 48 |
| Figure 24 - W.D.S and E.D.S line scan of oxygen content in an NdFeB magnet..... | 49 |
| Figure 25 - 3D confocal microscope Images for a Nd rich triple point imaged over 1 hour. | 51 |
| Figure 26 - 2D confocal images of a Nd-rich triple point imaged over 1 hour..... | 52 |
| Figure 27 – Height versus the square root of time for 6 Nd-rich triple points in dry and humid air. | 53 |
| Figure 28 - Raman results for a NdFeB magnet when compared with a Nd ₂ O ₃ reference..... | 55 |
| Figure 29 - Confocal Images of several score depths produced with a scalpel and a dremel tool on the surface of a NdFeB magnet. | 59 |
| Figure 30 - Mock flate plate assembly and temperature recording apparatus. | 63 |

Figure 31 - Mock flate plate assembly after hydrogen decrepitation. a) Entire assembly with line drawn on to indicate bend b) damaged magnet c) damaged magnet d) Uncoated magnet removed by hydrogen decrepitation e) Side view of assembly (the thickness of the plate was 0.8 cm).64

Figure 32 - Temperature data for the sensors positioned on the resin (sensor 1) and the centre of a surrounding magnet (sensor 2).65

Figure 33 - MagScan data prior to hydrogen decrepitation.....67

Figure 34 - MagScan data for post decrepitation.67

Figure 35 - Tiled optical image of an encapsulated NdFeB sample before (a) and after (b) hydrogen exposure.....70

List of Tables

| | |
|--|----|
| Table 1 -A comparison between the cgs system of units and mks system of units in the study of magnetism..... | 8 |
| Table 2- A summary of the five types of magnetism with their magnetic behaviour where M is Magnetisation and H is applied field. Zakotnik, 2004..... | 13 |
| Table 3- Magnetic properties of various $RE_2Fe_{14}B$ phases [Buschow et al., 1986] | 24 |
| Table 4 - High Temperature Oxidation of NdFeB Bulk samples. | 56 |
| Table 5 - Oxidation of NdFeB powdered samples..... | 57 |
| Table 6 - Average depth of score when scored with a scalpel and imaged with a confocal microscope at x50 magnification..... | 60 |
| Table 7 - Length measurements for the sample before and after exposure to hydrogen. | 70 |

Nomenclature

| | |
|---------------|---|
| at% | - Atomic Percent |
| B | - Magnetic Induction |
| BSI | - Back Scattered Image |
| $(BH)_{\max}$ | - Maximum Energy Product |
| B_r | - Remanence |
| EDS | - Energy Dispersive Spectroscopy |
| Fe_2B | - Ferro-boron |
| G | - Gauss |
| H | - Applied Field |
| H_2 | - Hydrogen |
| H_c | - Coercivity |
| HD | - Hydrogen Decrepitation |
| HDD | - Hard Disk Drive |
| HDDR | - Hydrogenation Disproportionation Desorption Recombination |
| HR-SEM | - High Resolution Scanning Electron Microscope |
| J | - Polarisation |
| $kA\ m^{-1}$ | - kilo Amps per metre |

| | |
|-------------------------|--------------------------------|
| kJ m^{-3} | - kilo Joules per metre cubed |
| M | - Magnetisation |
| MGOe | - Mega Gauss Oersted |
| M_s | - Saturation Magnetisation |
| Nd_2O_3 | - Neodymium Oxide |
| NdFeB | - Neodymium Iron Boron |
| NdH | - Neodymium Hydride |
| NdH_2 | - Neodymium Dihydride |
| Oe | - Oersted |
| ppm | - Parts Per Million |
| RE | - Rare Earth |
| SEI | - Secondary Electron Imaging |
| SEM | - Scanning Electron Microscope |
| SmCo | - Samarium Cobalt |
| T | - Tesla |
| T_c | - Curie Temperature |
| TEOS | - Tetra Ethyl Ortho Silicate |
| χ | - Magnetic Susceptibility |

| | |
|-----|---------------------------------|
| VCM | - Voice Coil Motor |
| VSM | - Vibrating Sample Magnetometer |
| wt% | - Weight Percent |
| WDS | Wave Dispersive Spectroscopy |

1. Introduction

Rare earth permanent magnets based upon neodymium-iron-boron (NdFeB) are used in a wide range of applications. These include electronic equipment such as hard disk drives and clean energy technologies such as generators in gearless wind turbines and electric motors in hybrid and electric vehicles. By using NdFeB magnets in wind turbine generators, it is possible to manufacture the device as a direct drive machine. This allows the blades to spin at the same speed as the generator, removing the need for a gearbox. This is an advantage for offshore wind turbines where it can be very expensive to replace the gearbox, which is the component most likely to fail.

If permanent magnet wind generators are introduced on a large scale (most are currently induction machines) this will require large quantities of rare earth materials; with each permanent magnet wind turbine containing around 0.5-0.75 tonnes per megawatt of rare earth permanent magnets (Gutfleisch, 2011). When this is coupled with the fact that many countries including the United Kingdom, the United States and China are installing large numbers of offshore wind turbines in order to meet their growing energy demands, then this will put considerable strain on the rare earth supply chain (Figure 1).



Figure 1 – World total installed capacity of wind turbines in MW. Gutfleisch, 2011.

China currently produces over 95% of the world's rare earth elements including neodymium, dysprosium

and samarium, which are used to make rare earth magnets. In 2006, China began to impose restrictions on the export of these materials with the quota being cut by 40% in 2010. The result of this was that the price of neodymium rose from around \$20/kg in 2009 to around \$200/kg in March 2012 peaking at \$450/kg in July 2011 ([www.metal-pages.com/metalprices/neodymium\[date\]](http://www.metal-pages.com/metalprices/neodymium[date]) accessed 04/12/12)). Not only has the material increased significantly in price and become difficult to source, but also the delivery times of the material have increased significantly which has caused big problems for end users of these materials.

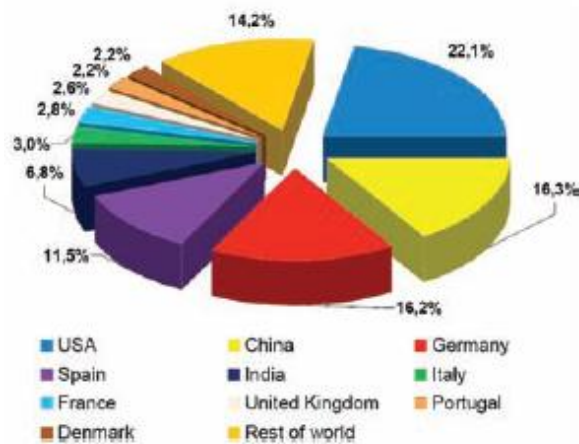


Figure 2 - Percentage of wind energy produced by countries worldwide. Gutfleisch, 2011.

The shortfall in rare earth material could be solved using various routes;

- Firstly, alternative technologies could be considered, for example using existing induction technology for wind turbines or electric vehicles. However, this would potentially result in a drop off in efficiency.
- New mines could be opened to increase the production of rare earth materials outside of China. However new mining operations can take up to 20 years to start up so this is a long-term solution.
- To develop a new substitute permanent magnetic material, use alternative magnetic materials or reduce the rare earth content of magnets. Researchers around the world have been searching

for an alternative for NdFeB since its discovery in 1984 without success. Although some current research is focused in this area (for example on MnB [Chinnasamy et al, 2012]). Some end users of NdFeB magnets have switched back to SmCo magnets. However, this is associated with a reduction in magnetic remanence and therefore the device will be less efficient. There are many workers around the world investigating the reduction of the neodymium and dysprosium content of NdFeB magnets (Gutfleisch et al, 2012). Although this work has proved successful, this will only help reduce the problem of supply.

- Another possible solution would be to recycle NdFeB magnets that are contained within electrical equipment. At present, there is no fully commercial activity on recycling of rare earth magnets worldwide. The Magnetic Materials Group (MMG) at the University of Birmingham is investigating the use of hydrogen to extract magnets from electrical goods and to then reprocess that material into new magnetic materials [Walton et al, 2012 & Zakotnik et al, 2009].

The current investigation proposes a method to recycle magnets and assemblies from medium to large scale devices such as generators and motors, which can be found in electric vehicles such as the Electric Smart Car. It can be difficult to remove these magnets as the magnets are magnetized and then glued into the assembly. Currently the only way to remove these magnets is to “chisel-off” the magnets from the rotor. This causes problems as the magnet material is still magnetised and will therefore stick to the remaining magnets. A further problem may be that chiselling the magnets may cause damage to the underlying shaft that could potentially be re-used.

The aim of this project is to investigate whether hydrogen gas can be used to remove NdFeB magnets from motor assemblies by breaking the magnets into a hydrided powder. The same technique will be used to selectively target magnets that have been damaged in operation or have been glued into the assembly in the wrong orientation by using masking agents to protect some of the magnets from reaction in hydrogen, the aim being to remove single/sections of magnet from an assembly without damaging the remaining substrate or magnets. In order to ensure no damage is caused to the

surrounding magnets and to the steel assembly the thermal and mechanical impact of the hydrogen treatment will be characterised. Several barrier coatings will be investigated to protect the NdFeB magnets from hydrogen decrepitation.

One of the challenges faced by recycling of rare earth magnets is the starting condition of the scrap material. Scrap magnets are likely to have a considerable surface oxide that could potentially prevent the initiation of hydrogen decrepitation on the magnets surface. Therefore as part of this project, the growth rate and form of oxides on sintered NdFeB magnets will be analysed using a confocal laser microscope combined with Raman Spectroscopy. The effect of surface oxides on the initiation of hydrogen decrepitation will be investigated as well as the impact of surface damage to those oxide layers.

2. Literature Survey

The first recorded discovery of magnetism dates back 4000 years ago to the Chinese who discovered Lodestone based upon Fe_3O_4 . The name Lodestone comes from the Latin 'to lead', this is because the first application of lodestone was in a compass.

The next milestone in the development of the magnet was by William Gilbert in the 16th century who wrote 'De Magnete'. He theorised that the Earth possessed a magnetic field and this was the reason for the compass needle pointing in the northerly direction. In this work, he also proposed that there were three ways in which a steel compass needle could be magnetised. The first was to touch the needle with a lodestone. The second was to cold draw the steel when it is in the north-south direction and the third was by prolonged exposure to the earth's magnetic field whilst in the north/south direction.

In the 18th century, the first permanent magnets were developed which were based upon Magnetic Carbon Steels. These steels, which are commonly alloyed with tungsten or chromium and heat-treated, have a much higher energy product than lodestone.

Christian Oersted discovered the effects of electrical currents on magnetic fields in the 19th century. He found that when a wire carrying an electrical current was brought into close proximity with a compass, there would be a deflection of the compass needle. Andre Marie Ampere also discovered that when two wires were placed in parallel to one another carrying a current, they would attract each other if the current was in the opposite direction and repel each other if the current was in the same direction.

It was during the 20th century that permanent magnet materials started to be developed further and used in various applications. In 1917, Japanese investigators Honda and Takagi discovered a steel based magnet that contained 30-40% cobalt plus some tungsten and chromium, this produced a magnet with a higher coercivity than had been seen before of 18.3 kA/m with an energy product of 8 kJ/m³ (Cullity, 2009).

In 1931, Alnico magnets were introduced by T. Mishima in Japan. (Cullity, 2009). These magnets were comprised of Al, Ni and Co and were therefore called the 'Alnico' magnets. Due to the shape anisotropy of the grains they had a much higher coercivity than the steel magnets that were used before (32 kA/m) and have a high temperature stability and Curie temperature (800°C). Due to this property the Alnico magnets are still used for some niche applications today.

The ferrites were the next development in permanent magnets and were first discovered in the 1950's. These magnets are commonly known as ceramic magnets and have a relatively high coercivity value (100-300 kA/m). However as the magnets demonstrate ferromagnetic behaviour they have a low remanence (200-500 mT) and this therefore hinders the maximum energy product. The ceramic magnets are typically based upon strontium ferrite ($\text{SrFe}_{12}\text{O}_{19}$), barium ferrite ($\text{BaFe}_{12}\text{O}_{19}$) or cobalt ferrite (CoFe_2O_4) and are very cheap and relatively easy to process (McGuinness, 1989).

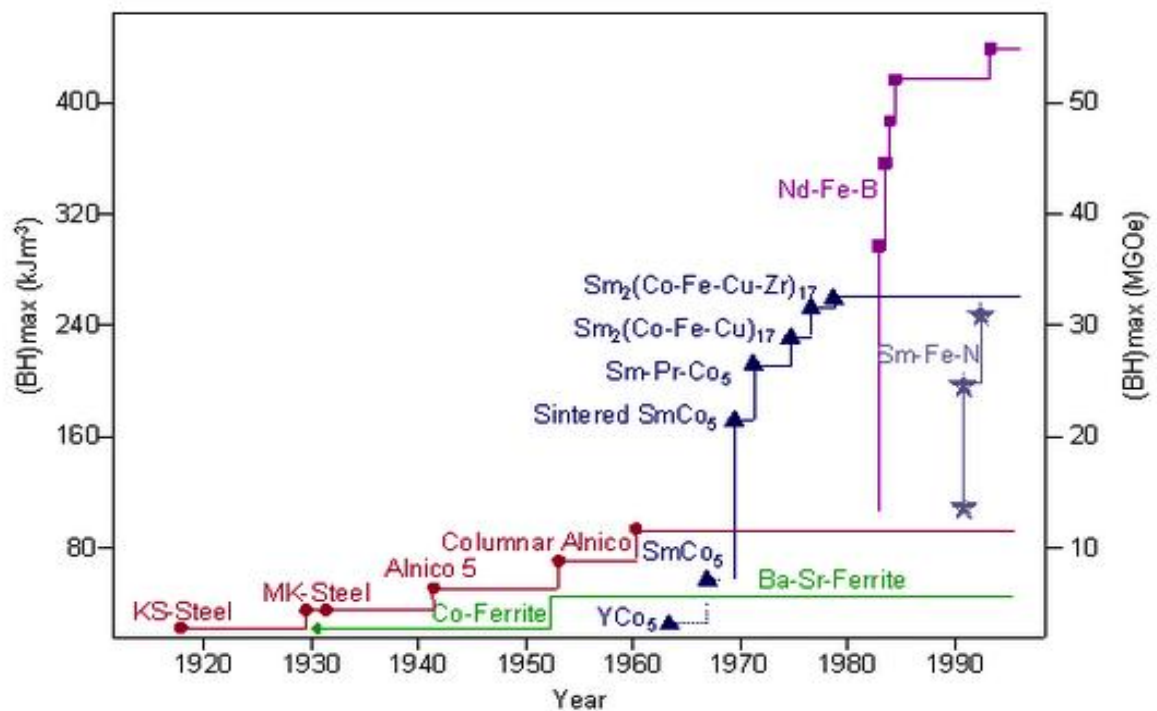


Figure 3 - A history of permanent magnet development in the 20th Century - http://www.magnets.bham.ac.uk/magneticmaterials/historupdate_y.shtml <viewed on the 29/06/2011>

There was a realisation that in order to gain higher coercivity values, higher levels of magnetic anisotropy

must be obtained (McGuinness, 1989). This could be achieved by implementing a material that had an anisotropic crystal structure, such as a hexagonal or tetragonal crystal structure. During the 1960's, the first rare earth magnets were developed by Strnat (1967) based upon SmCo as shown in Figure 3. These permanent magnets contained the rare- earth element Samarium and had a much higher energy product than other competing magnets at the time. The most useful was SmCo₅ that had high magnetocrystalline anisotropy and therefore high coercivity. These magnets were first produced by polymer bonding; however, they were then sintered in order to produce fully dense magnets that had a higher maximum energy product (Ormerod et al, 1997). These materials have a high coercivity and an energy product that is only bettered by NdFeB magnets. However, they have traditionally been expensive due to the relative scarcity of Samarium when compared to other rare earth materials, and the high value of cobalt (Ormerod et al, 1997).

There are two forms of samarium cobalt magnets, SmCo₅ and Sm₂Co₁₇. SmCo₅ has a hexagonal crystal structure and SmCo₅ magnets have been reported with energy products as high as 159 kJ/m³. The second form is Sm₂Co₁₇. Song et al [2009] reported that there are three kinds of crystal structures present at room temperature in Sm₂Co₁₇; rhombohedral and two hexagonal type structures. Sm₂Co₁₇ has a very fine microstructure consisting of bands of SmCo₅ separated by regions of Sm₂Co₁₇ (Cullity, 2009).

NdFeB magnets were discovered in 1983 by Sumitomo Special Metals in Japan and displayed very high energy products. This brought them into competition with the SmCo magnets that were the dominant permanent magnets throughout the 1970's (Cullity, 2009). During the 1980's, two different processing routes were discovered for the NdFeB magnets. Firstly there was the powdered processing route by Sagawa et al (1984) and secondly the melt quenching route which was discovered by Croat et al in 1984.

NdFeB magnets possess the highest energy product of all the permanent magnets with theoretical energy products of 509 kJ/m³ (Popov, 2010). However, these magnets suffer from two disadvantages over other permanent magnetic materials; they have a relatively low Curie point which is 312°C (Sagawa,

1984) and low corrosion resistance (Coey, 1995).

2.1. Properties of Permanent Magnetic Materials

The magnetic field developed in a permanent magnet originates from the orbital motion and spins of the electrons. In atoms with complete electron shells the net effect of the electron motion is countered by one of opposing polarity and there is therefore no contribution to the magnetic moment of the atom. However, in atoms without a full electron shell there may be an imbalance in polarity that has a contribution to the magnetic moment of the atom.

There are two main systems of units in the study of magnetism; these are the mks (metres-kilograms-seconds) system and the cgs (centimetres-grams-seconds) system. The mks system is most commonly used and it has been adopted as the S.I. units. However, the cgs system is popular as there is a closer numerical equivalence between the magnetic induction (B) and the applied field (H). A comparison between the two unit systems is shown in Table 1.

Table 1 -A comparison between the cgs system of units and mks system of units in the study of magnetism.

| Quantity | Gaussian (cgs units) | S.I. Units | Conversion factor (cgs to S.I.) |
|-------------------------------------|-------------------------|----------------------|---------------------------------|
| Magnetic Induction (B) | G | T | 10^{-4} |
| Applied Field (H) | Oe | $A\ m^{-1}$ | $10^3 / 4\pi$ |
| Magnetisation (M) | $emu\ cm^{-3}$ | $A\ m^{-1}$ | 10^3 |
| Magnetisation ($4\pi M$) | G | - | - |
| Magnetic Polarisation (J) | - | T | - |
| Specific Magnetisation (σ) | $emu\ g^{-1}$ | $J\ T^{-1}\ kg^{-1}$ | 1 |
| Permeability (μ) | Dimensionless | $H\ m^{-1}$ | $4\pi \cdot 10^{-7}$ |
| Relative Permeability (μ_r) | - | Dimensionless | - |
| Susceptibility (χ) | $emu\ cm^{-3}\ Oe^{-1}$ | Dimensionless | 4π |
| Product of $B \cdot H$ | M G Oe | $k\ J\ m^{-3}$ | $10^2 / 4\pi$ |

The magnetic behaviour of all materials can be divided into 5 main categories: paramagnetic, diamagnetic, ferromagnetic, anti-ferromagnetic, and ferri-magnetic. These materials can be identified by their susceptibility (χ in table one), which is described below.

$$\chi = \frac{M}{H}$$

Equation 1

Where M is the magnetisation of the material with units ($\text{JT}^{-1}\text{m}^{-3}$). This is a measure of the magnetic moment per unit volume. H is the applied field with units (Am^{-1}). The susceptibility of a material describes its response to an applied field.

Another important factor that must be considered in a magnet is the magnetic induction (B). This can be described by.

$$B = \mu_0(H + M) \quad \text{Equation 2}$$

The magnetic induction (B) describes the total magnetic flux through a unit cross sectional area. Where μ_0 is the permeability of free space. M is the magnetisation of the material with units ($\text{JT}^{-1}\text{m}^{-3}$). H is the applied field with units (Am^{-1}).

The magnetic polarisation (J) is another useful parameter and can be used in the S.I. unit system to express the magnetisation of a sample in Tesla.

$$J = \mu_0 M_s \quad \text{Equation 3}$$

Saturation magnetism M_s is an important measure in magnetism as it describes the maximum field that can be generated by a material.

2.2. Types of Magnetism

2.2.1. Paramagnetism

Paramagnetism occurs when atoms have randomly orientated magnetic moments when a magnetic field is applied. A small positive magnetisation is produced in the direction of an applied magnetic field. The interactions are very small when compared with the thermal energy. This causes the alignment of the atoms to be random and fluctuating (J.C. Anderson, 1990). There is a very low susceptibility associated with paramagnetism that is lost when the magnetic field is removed.

2.2.2. Diamagnetism

When a magnetic field is applied to a diamagnetic material, there is a weak magnetisation in the direction opposite to that of the applied magnetic field. The susceptibility of these materials is small and negative. Ohring (1995) described how Diamagnetism is a manifestation of Lenz' Law when it is applied to a current loop. The motion of the electrons can be described as a current loop and if a magnetic field is applied to the loop then the current flows and a magnetic field occurs which counteracts the applied field. This effect can be seen in all materials; however, it is often overshadowed by other contributions due to the low susceptibility of the diamagnetic effect. Diamagnetism is the most common type of magnetism to arise in elemental materials, as demonstrated in the periodic table in Figure 4.

2.2.3. Ferromagnetism

There are only three ferromagnetic elements at room temperature, nickel, cobalt and iron (Figure 4). All of these elements have permanent magnetic moments that remain when a magnetic field is removed as can be seen in

Table 2. When a magnetic field is applied to a ferromagnetic material, there is an alignment of the magnetic moments with the magnetic field. These materials have large positive susceptibility.

Ferromagnetic materials are subject to the Curie-Weiss law that states that the susceptibility of a ferromagnet is inversely proportional to the temperature difference from the Curie point (McGuinness, 1989). This is due to the disordering effect of the thermal energy on the lattice that causes the alignment of the atomic moments to be reduced (J.C. Anderson, 1990). The Curie temperature is the temperature at which the forces trying to align the magnetic moments are not strong enough to overcome the effect of the thermal disordering. The curie temperature of a material is explained by the equation below.

$$\chi \sim \frac{C}{T - T_c} \quad \text{Equation 4}$$

Where C is a Curie constant for the material, T is the absolute temperature and T_c is the Curie

temperature in Kelvin.

2.2.4. Ferrimagnetism

The origin of Ferrimagnetism arises from magnetic ions located within the sub lattices that have different magnetisations and spin orientations (Ohring, 1995). This causes the magnetic moments to have an anti-parallel alignment, with alternate atoms having magnetic moments pointing in opposite directions, AND with the strength in each direction being unequal (Jakubovics, 1994). Therefore, these moments do not cancel each other out (J.C. Anderson, 1990). The susceptibility of ferrimagnetic material is large and in the positive direction. These materials are useful as they are often electrical insulators.

2.2.5. Anti-ferromagnetism

These materials have a small positive susceptibility that is similar in magnitude to that of paramagnetic materials. In Antiferromagnetic materials, the direction of the electron spins alternate up and down in adjacent atoms (Ohring, 1995). This anti-ferromagnetism is subject to the Néel temperature which is the temperature above which the thermal disordering becomes great enough for an anti-ferromagnetic or ferromagnetic material to become paramagnetic.

2.3. Magnetocrystalline Anisotropy

Most permanent magnetic materials have a preferred direction of magnetisation known as the easy axis of magnetisation. This is due to spin orbit coupling with the crystal lattice. In some materials there is only one preferred axis as in cobalt. This is called uniaxial magnetocrystalline anisotropy. Anisotropy can also be developed by changing the microstructure of a material, for example long particles/grains will demonstrate an easy axis of magnetisation along the long axis of each particle/grain.

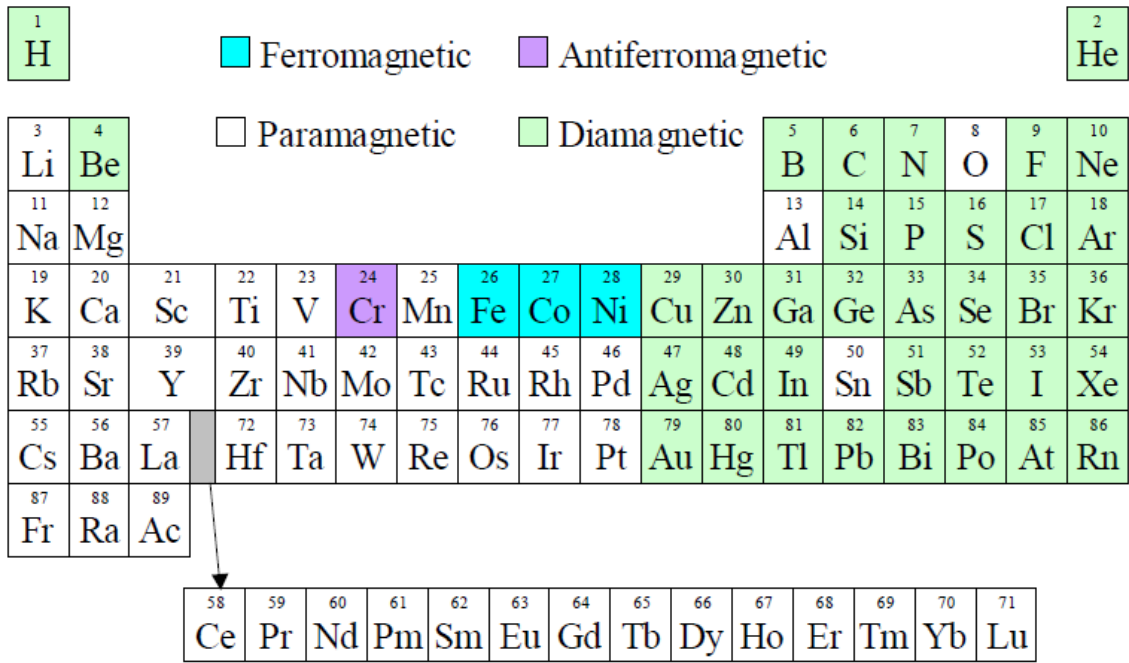
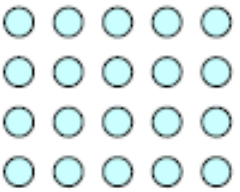
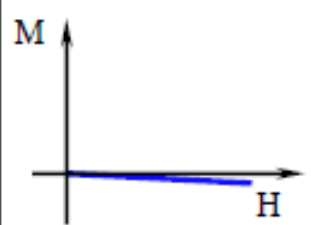
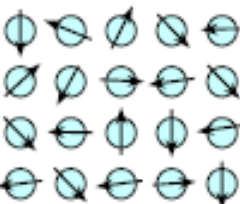
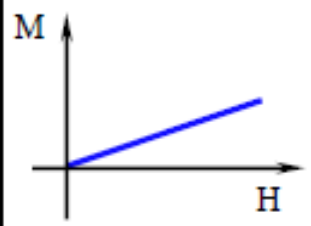
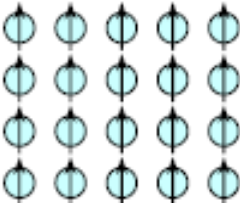
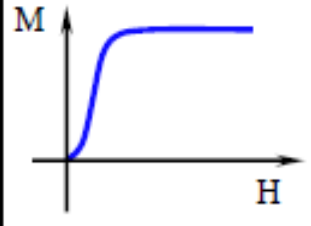
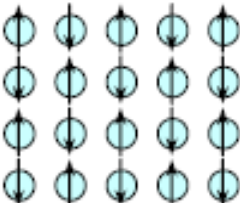
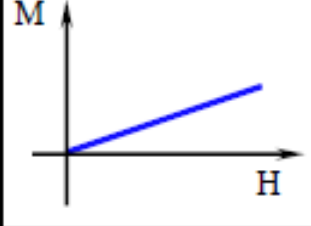
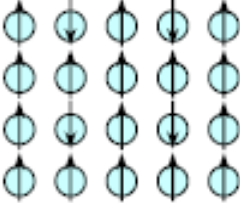
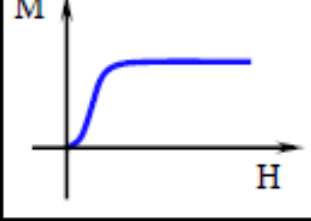


Figure 4 - A periodic table showing the elements that are ferromagnetic, paramagnetic, antiferromagnetic and diamagnetic. Zakotnik 2004.

Table 2- A summary of the five types of magnetism with their magnetic behaviour where M is Magnetisation and H is applied field. Zakotnik, 2004.

| Type | Atomic / Magnetic Behaviour | |
|---------------------|---|---|
| Dia-magnetism |  <p>Atoms have no magnetic moment</p> |  |
| Para-magnetism |  <p>Atoms have randomly oriented magnetic moments</p> |  |
| Ferro-magnetism |  <p>Atoms have parallel aligned magnetic moments</p> |  |
| Antiferro-magnetism |  <p>Atoms have anti-parallel aligned magnetic moments</p> |  |
| Ferri-magnetism |  <p>Atoms have mixed parallel and anti-parallel aligned magnetic moments</p> |  |

2.4. Magnetic Hysteresis

A ferromagnetic material will demonstrate spontaneous magnetisation. However, in some instances no net magnetisation is produced. Domains are regions in the material where the dipole moments are aligned in one direction. If all the domains in a ferromagnetic material are aligned in one direction then the sample will have a net magnetisation, however, if there is a random alignment of the domains then the net magnetisation can be zero.

When a magnetic field is applied to a non-magnetised ferromagnetic material then the domains that are orientated in the same direction as the applied field will grow preferentially to those in opposing directions until the saturation magnetisation is reached. A permanent magnetic material will retain its internal magnetism when the applied field is subsequently reduced to zero. This is due to the limitation of the growth or the movement of domains (see coercivity mechanisms). The response of a ferromagnetic material to an applied field can be classified by its hysteresis loop (Figure 5).

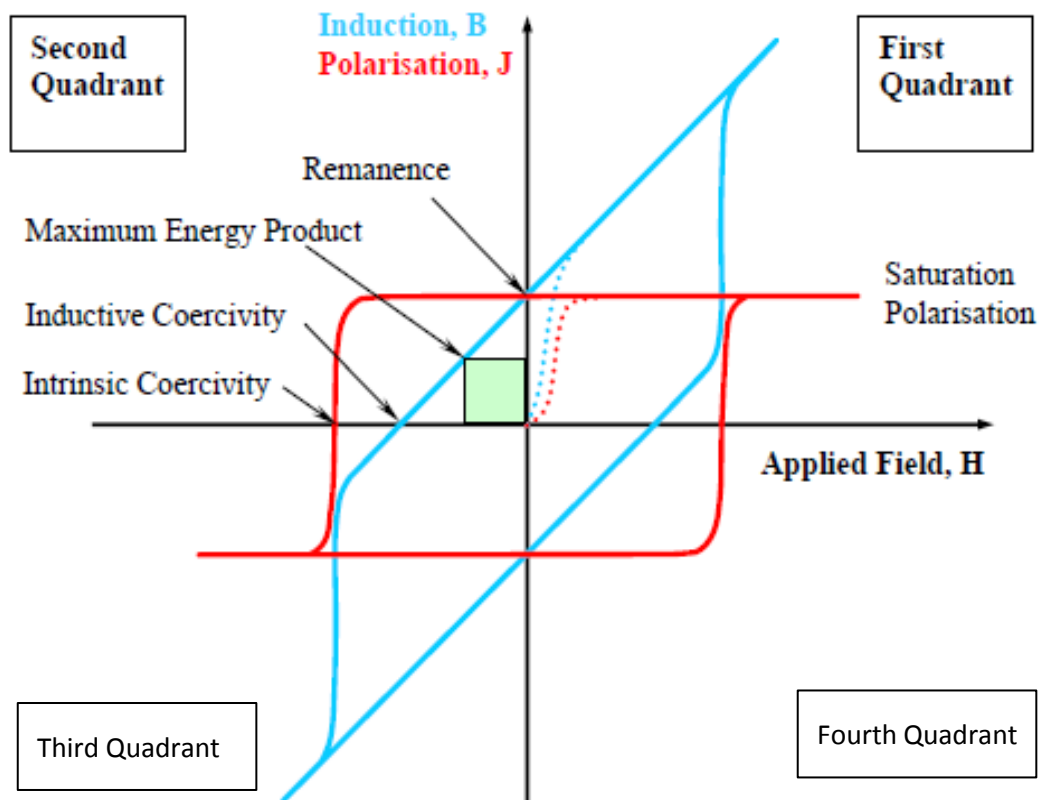


Figure 5 - Hysteresis Loop for a ferromagnetic material.

When the applied field is removed ($H=0$) the polarisation that remains in the magnet once the applied field is removed is known as the remanence (B_r or J_r) [Figure 5]. A negative field is then applied to the sample that reduces the polarisation (red line) of the material to zero; the magnitude of this negative applied field is known as the intrinsic coercivity [Figure 5]. The inductive coercivity is determined by the field required to reduce induction to zero. The blue line on Figure 5 displays the induction curve which is a plot of the total flux in the magnet.

The maximum energy product is the product of B and H and is a measure of the useful work that a magnet can perform. It is measured by the largest square that will fit under the induction line in the second quadrant of the hysteresis loop. The maximum energy product is an important measure in the field of magnetism as it is used as a figure of merit. The higher the maximum energy product the smaller the magnet required to do the same amount of work.

2.5. Coercivity mechanisms

The resistance to demagnetisation or coercivity is an important property in magnetic materials and is linked to the movement of domain walls and the rotation of the magnetisation vector (Cullity, 2009). To produce a material with high coercivity it is therefore necessary to either prevent nucleation of reverse domains or the movement of domain walls by introducing pinning sites. There are three main coercivity mechanisms linked to the microstructure of a material.

1. *Nucleation of reverse domains* – The nucleation of reverse domains commonly occurs at inhomogeneities such as irregularities in the grain boundaries of the material (Cullity, 2009). These inhomogeneities provide a nucleation point for reverse domain, and once the domain has been formed, it can grow unimpeded. The grain boundaries in a material should be as smooth as possible. Heat treatments can be utilised to reduce inhomogeneities and smooth the grain boundaries. It is important to ensure that the grains are isolated from each other so that reverse domains cannot spread between grains.
2. *Domain wall pinning*- The coercivity in a magnetic material can also be controlled by domain wall pinning. In this effect, the movement of magnetic domains is impeded by inclusions or dislocations in the crystal structure of a material; thus impeding the motion of the domain wall. An external field is required to overcome the pinning field, leading to an increase in coercivity of the material.
3. *Single domain particle grains* – When the grain size of a ferromagnetic material is reduced it is possible to produce single domain particles. This occurs at a size when the grain is so small that the decrease in magnetostatic energy (forces arising from dipole-dipole interaction) is smaller than the energy associated with a domain wall. A reverse domain cannot therefore nucleate and grow in one of these grains. The magnetisation has to flip from one direction to another.

High coercivities can be achieved in materials that demonstrate uniaxial magnetocrystalline anisotropy. This is an intrinsic property of the material. Extrinsic properties can also play a role in coercivity mechanisms. This is due to the fact that domains can interact with the microstructure of a permanent magnet. As such, by modifying the microstructure of a permanently magnetic material it is possible to influence coercivity.

2.6. NdFeB

NdFeB sintered magnets consist of an $\text{Nd}_2\text{Fe}_{14}\text{B}$ matrix phase and an Nd-rich grain boundary phase, as shown in the scanning electron microscope image in Figure 6. An $\text{Nd}_{1+x}\text{Fe}_4\text{B}_4$ phase is also present, however, it can not be observed in the figure.

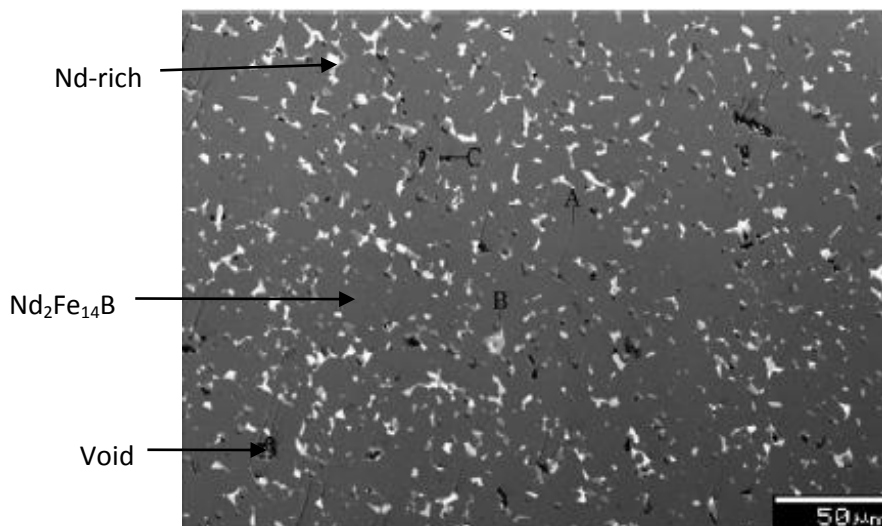


Figure 6 – SEM image of sintered NdFeB. Zakotnik (2009).

2.6.1. $\text{Nd}_2\text{Fe}_{14}\text{B}$

Herbst (1984) used neutron diffraction to characterise the crystal structure of $\text{Nd}_2\text{Fe}_{14}\text{B}$. In the same year Givord (1984), Shoemaker (1984) and Boller and Oesterreicher (1984) used x-ray diffraction to determine its structure. The crystal structure of $\text{Nd}_2\text{Fe}_{14}\text{B}$ is shown in Figure 7. $\text{Nd}_2\text{Fe}_{14}\text{B}$ has a tetragonal structure and contains 68 atoms with lattice parameters of $a=0.88\text{nm}$ and $c=1.22\text{nm}$ (Skulj, 2005). The Nd atoms are arranged in an alternating large and small rhombus in $z=0$ and $z=0.5$ whilst the Fe atoms are arranged

in a planar net of slightly deformed hexagons and triangles (Givord, 1984). The boron site is shown to be 4g.

The $\text{Nd}_2\text{Fe}_{14}\text{B}$ phase is the only ferromagnetic phase in an NdFeB magnet. The substitution of the Fe atoms with the Nd atoms causes high anisotropy in the structure, whilst Fe produces high saturation magnetisation. Therefore, the combination of these properties leads to magnets with high remanence and coercivity.

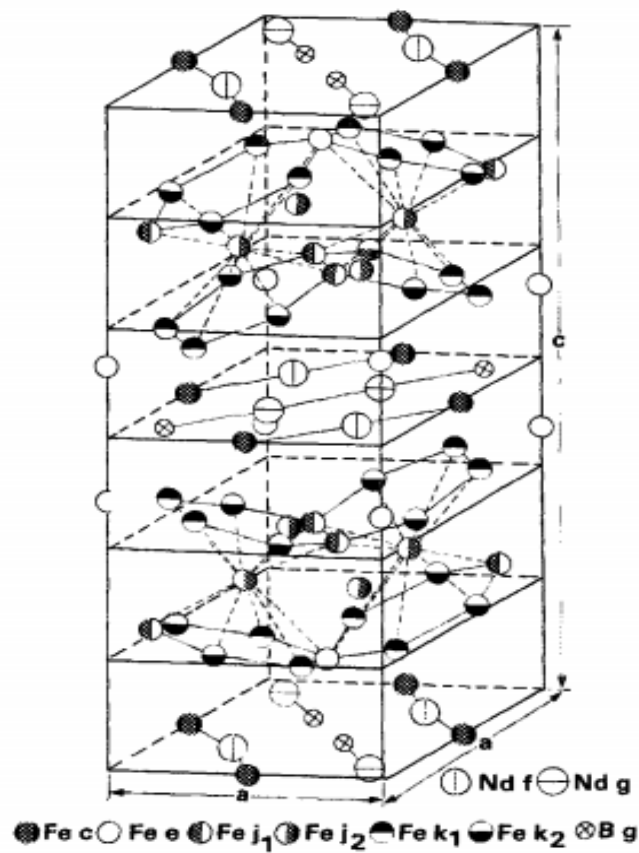


Figure 7 - Crystal Structure of $\text{Nd}_2\text{Fe}_{14}\text{B}$ – (Herbst, 1985).

2.6.2. $\text{Nd}_{1+\epsilon}\text{Fe}_4\text{B}_4$

Givord (1985) describes a second phase in the NdFeB system to be $\text{Nd}_{1+\epsilon}\text{Fe}_4\text{B}_4$. This phase is paramagnetic when it is at room temperature due to the Curie temperature of this phase being only 15 K

(Sun, 2012).

2.6.3. Nd-rich phase

The Nd-rich phase forms as a eutectic at the grain boundaries in the NdFeB system. Fidler (1987a) has shown that the Nd-rich phase contains 85 at% Nd with the remaining 15 at% comprising of Fe with a small amount of B. The crystal structure is usually double hexagonal close packed (McGuinness, 1989).

The phases present in Nd-rich grain junctions are described by Woodstock, 2012 to also contain crystalline oxides such as NdO, Nd₂O₃ and NdO₂. If other phases are present in the material such as Pr and Dy then phases such as (Nd,Pr,Dy)₂O₃ are formed.

The Nd-rich phase is a very important phase in this material and can have a large effect on the final magnetic properties of the NdFeB magnet. This phase smooths the grain boundaries between the Nd₂Fe₁₄B grains which reduces the inhomogeneities which give rise to reverse nucleation sites, therefore increasing the coercivity of the material. It also isolates each individual Nd₂Fe₁₄B grain which prevents exchange coupling between grains in close proximity to one another again increasing the coercivity of the magnet.

A finely distributed Nd-rich phase is required for a magnet with good properties, this will have the effect of increasing liquid phase sintering which produces a denser magnet with a smaller grain size, therefore imparting superior magnetic properties.

2.7. Processing of NdFeB magnets

NdFeB magnets can be manufactured in two forms, either as fully dense sintered magnets or as polymer bonded magnets.

2.7.1. Resin Bonded Magnets

Resin bonded magnets contain NdFeB powder suspended in resin binder (typically an epoxy resin or PTFE). Polymer bonded magnets use nanocrystalline powders manufactured by a melt spinning process

or by a high temperature hydrogen processing route known as HDDR (Hydrogen Disproportionation Desorption and Recombination). Polymer bonded magnets are advantageous as they are inexpensive and are easy to form into complicated shapes by processing routes such as injection moulding. These magnets are produced by mixing the powder with the resin, aligning the powder in a magnetic field and then pressing. Bonded magnets are not suitable for the recycling processes described in this work and as such, they are not covered in detail here.

2.7.2. Sintered NdFeB magnets

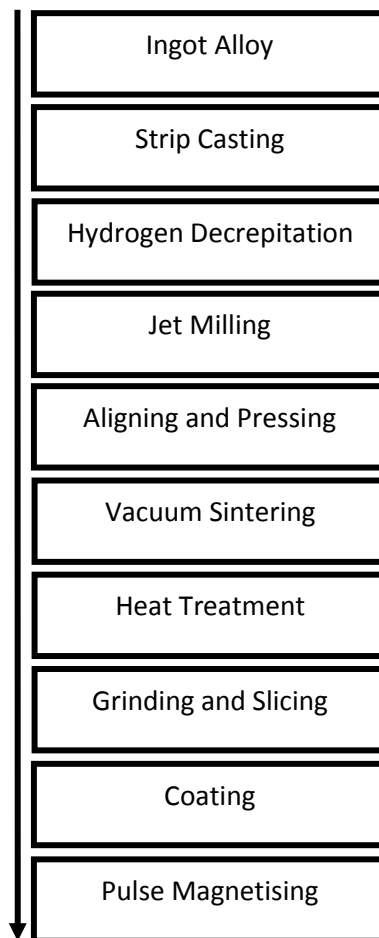


Figure 8 - Production of rare-earth magnets via sintering.

Fully dense sintered magnets are produced via a powder metallurgical process, as shown in Figure 8. The first step in the process is to melt the elements in a vacuum furnace (Kaneko, 2006). The vacuum furnace is used because it limits the exposure of the alloy to oxygen, which would have the effect of introducing

impurities and lowering the coercivity of the magnet. The NdFeB is then typically strip cast in order to form NdFeB flakes. Strip casting is a process where the molten material is poured onto a water cooled copper wheel, causing the material to cool very quickly. The advantage of a high cooling rate is that α -Fe does not form in the material which would reduce the crushability of the NdFeB and lead to reduced alignment and therefore magnetic properties.

The next steps in the powder metallurgical process is to process the cast alloys in hydrogen (hydrogen decrepitation (HD)). This breaks up the material to produce a hydrided powder. Harris (1987) showed that when NdFeB type alloys are introduced in a hydrogen atmosphere at atmospheric pressure and room temperature, the Nd rich phase at the grain boundaries initially absorbs the hydrogen forming $\text{NdH}_{2.7}$, which leads to an expansion in the lattice and as a result intergranular cracking occurs. An exothermic reaction ensues which then allows hydrogen to be interstitially absorbed by the $\text{Nd}_2\text{Fe}_{14}\text{B}$ matrix grains. This causes a 5% expansion in the matrix grains which causes transgranular cracking.

The use of hydrogen decrepitation is associated with a 25% cost saving when compared to the production of sintered magnets without the use of hydrogen decrepitation (McGuinness, 1986). It is advantageous as the hydrogen decrepitation is carried out in a reducing atmosphere; therefore, this limits the oxidation of the material. The hydrogen decrepitation also allows for shorter milling times, as the decrepitated material is highly friable.

Once the hydrogen decrepitation is complete, the material is jet milled to a particle size of approximately $3\mu\text{m}$ (Kaneko, 2006). (Li, 2006) demonstrated that jet milling is one of the most important stages in the processing of magnets and therefore must be controlled carefully. In this stage, the aim is to achieve a narrow particle size distribution and a small particle size. Ideally, each particle should contain a single grain of $\text{Nd}_2\text{Fe}_{14}\text{B}$ so that full use can be made of the magnetocrystalline anisotropy demonstrated by this material. This can be achieved by; optimising the fluidisation in the chamber, ensuring the gas pressure is accurate and ensuring that there is no over milling (Li, 2006).

The powder is then aligned in a magnetic field and pressed into green compacts. The c-axes of the $\text{Nd}_2\text{Fe}_{14}\text{B}$ single grained particles then align with the applied magnetic field. This alignment is important as it can have a large effect on the $(\text{BH})_{\text{max}}$ value of the final magnet. Perfect alignment will occur when the particles are single crystals and uniform in shape. Therefore, their alignment is unconstrained and near perfect alignment can be achieved. Finally, the green compacts are sintered at around 1000°C in a vacuum furnace to create a fully dense product.

2.8. Oxidation and corrosion of NdFeB magnets

In service, sintered NdFeB magnets are likely to have been exposed to the atmosphere and as a result, the magnets will possess a surface oxide, which forms readily under these conditions [Kim, 1987]. The presence and degree of surface oxide layers on the magnets will vary and could influence the onset of decrepitation. This was observed by workers at the University of Birmingham, who found that in some instances hydrogen decrepitation cannot be used as a recycling tool without first pre-damaging the oxide present on the magnet surface [Internal Communication, 2011].

Further characterisation of the atmospheric oxidation of NdFeB magnets, particularly in the early stages, is required to understand how hydrogen interacts with NdFeB surfaces and initiates the decrepitation process.

The existing literature relates predominantly to the oxidation of powdered NdFeB samples [Osawa et al, 1992; Higgins et al, 1987], gravimetric measurements of corrosion/oxidation phenomena in solid samples at room temperature [Tenaud et al, 1990, Kim et al, 1987] or high temperature [$> 250^\circ\text{C}$] oxidation of solid NdFeB samples [Edgley et al, 1997].

Sintered NdFeB magnets have a three phase microstructure: the major phase being the $\text{Nd}_2\text{Fe}_{14}\text{B}$ [Φ -phase] matrix. There is also a lesser amount of Nd-rich grain boundary regions and a small amount of $\text{Nd}_{1.1}\text{Fe}_4\text{B}_4$ [η -phase]. Studies of the oxidation and corrosion of NdFeB have sought to relate the observed degradation mechanisms and corrosion/oxidation products to these salient microstructural features of

NdFeB.

Tenaud et al [1990] found that sintered NdFeB magnets degraded in 80°C/90% humidity conditions by the rapid formation of $\text{Nd}(\text{OH})_3$ in the grain boundary areas. Jacobson et al [1987] analysed the oxidation product formed at 20-50°C in atmospheric conditions and found it consisted mainly of iron oxides/hydroxides with small amounts of neodymium oxides. Jacobson et al [1987] summarised the effects of oxygen content on the corrosion stability of NdFeB magnets by noting that the magnetic properties are gradually lost due to the oxidation of the Nd-rich phases at the grain boundaries.

In summary the low temperature studies of sintered NdFeB magnets oxidised in air indicate that:

- In humid conditions the degradation of magnetic properties is rapid and proceeds by the formation of $\text{Nd}(\text{OH})_3$ and is strongly influenced by the specific composition of the magnet and trace amounts of environmental contamination, notably chlorides which results in hydrogen decrepitation.
- For dry air at low temperature, whilst the rates are lower than in the presence of humidity, the mechanism of the oxidation of the matrix phases remains unidentified.
- In several studies of the oxidation of NdFeB in dry air, the neodymium oxide observed is assumed to be associated with the Nd-rich areas of the grain boundaries, but no direct observations have been made.

2.8.1. Surface finish

There is a strong effect of the surface finish on the oxidation rates of the magnets and therefore it is very important to control this when studying the oxidation of NdFeB (Kim, 1987). There is a reduction in oxidation rate as the surface finish becomes smoother (Skulj, 2005). Rough and contaminated surfaces will have a much higher oxidation rate than clean smooth surfaces. This also has an effect on the distribution of the oxidation products. There will be an even distribution when the surface is smooth and

free from contaminants and a much more varied distribution for rough surfaces.

2.9. Additions to NdFeB

Modern day NdFeB magnets contain a variety of additions, which change the properties of the base alloy. Table 3 displays the magnetic properties of various additions to NdFeB magnets.

Table 3- Magnetic properties of various $RE_2Fe_{14}B$ phases [Buschow et al., 1986]

| $RE_2Fe_{14}B$ (R =) | Curie Temperature (T_c) (K) | Saturation Magnetisation (J_s) (T) | Anisotropy Constant (K_1) (MJ/m ³) | Anisotropy Field (Ha) (kA/m) |
|--------------------------|---------------------------------------|--|--|------------------------------------|
| Y | 571 | 1.38 | 1.06 | 1592 |
| La | 516 | 1.38 | - | 1592 |
| Ce | 533 | 1.17 | 1.7 | 2387 |
| Pr | 565 | 1.56 | 5.6 | 6923 |
| Nd | 588 | 1.60 | 5.0 | 5332 |
| Sm | 618 | 1.50 | -12 | - |
| Gd | 660 | 0.84 | 0.67 | 1989 |
| Tb | 629 | 0.70 | 5.9 | 17507 |
| Dy | 593 | 0.71 | 4.5 | 11937 |
| Ho | 574 | 0.81 | 2.5 | 5968 |
| Er | 557 | 0.90 | -0.03 | - |
| Tm | 540 | 1.15 | -0.03 | - |
| Lu | 539 | 1.17 | - | 2070 |

2.9.1. Dysprosium

Additions of dysprosium to NdFeB magnets act to increase the coercivity. This is due to the fact that Dy has a high anisotropy. The Nd in the matrix phase is substituted by Dy to form $Dy_2Fe_{14}B$. $Dy_2Fe_{14}B$ has a larger anisotropy field than $Nd_{14}Fe_2B$ ($Nd_{14}Fe_2B$ having a field of 7.6T and $Dy_2Fe_{14}B$ demonstrating an anisotropy field of 15.8T (Bai, 2007)). The dysprosium content of NdFeB magnets can vary significantly depending upon the coercivity and thermal characteristics required by the application. For example, a Toyota Prius motor that generates a significant amount of heat contains magnets with a Dy content of around 6-8% (of the rare earth content). Whereas a voice coil magnet in a hard disk drive will typically only contain 0.5%. The graph in Figure 9 displays the typical applications of magnets with varying Dy

contents and Figure 10 displays the effect of dysprosium additions on the magnetic properties.

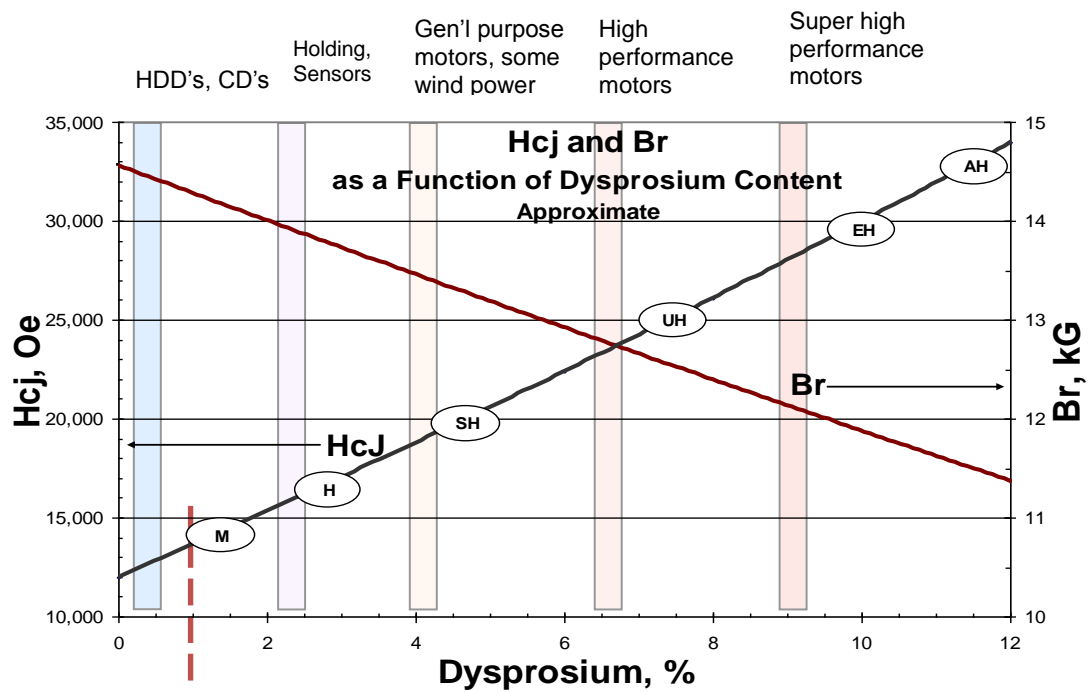


Figure 9 – The effect of dysprosium content on the remanence and coercivity of NdFeB magnets and the typical applications of these materials.

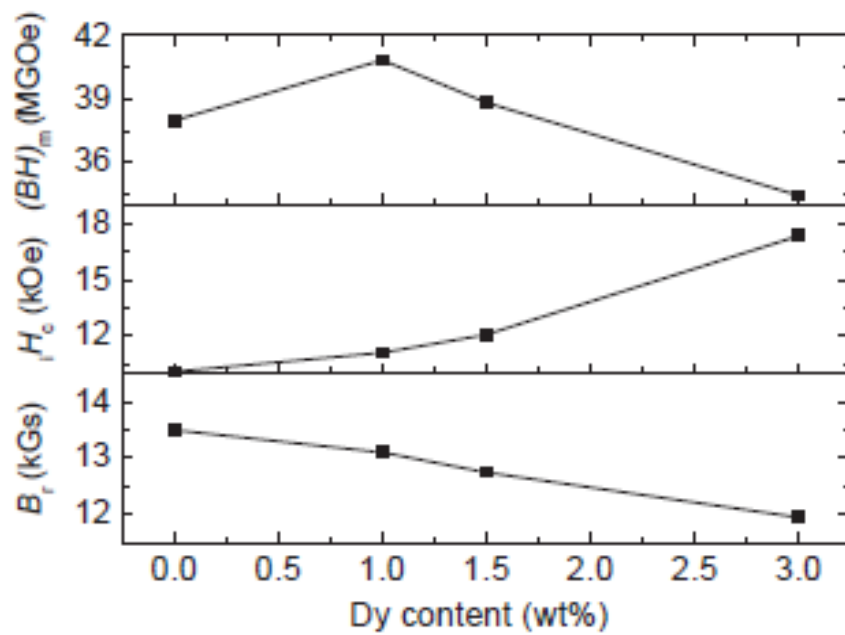


Figure 10 - The effect of Dy content on the magnetic properties of NdFeB. It can be observed that there is an improvement in coercivity, a reduction in remanence and an increase in BHmax up to 1 wt % Dy content. (Yu, 2004).

The second way in which Dy additions can increase the coercivity of NdFeB is by suppressing the separation of α -Fe branch crystals when the melt is solidifying. This has the effect of ensuring the grains are small, fine and uniform in shape which reduces surface defects in the grains. These factors all contribute to an increased coercivity as the Dy content is increased. This will also give an improvement in Curie temperature, as there is a link between coercivity and Curie temperature. (Bai, 2007).

However the drawback of using Dy additions to improve coercivity and therefore temperature resistance is that there will be a reduction in the saturation magnetisation of the magnet and therefore there will be a reduction in $(BH)_{\max}$ due to replacement of Nd with Dy. Dy is also expensive and therefore the quantity of Dy used is usually limited in all but the most high performance applications as shown in Figure 9.

2.9.2. Cobalt

Cobalt can be added to NdFeB to improve its Curie temperature (Kim, 1996). When cobalt is added to NdFeB it substitutes into the matrix and replaces iron to form the $\text{Nd}_2(\text{Fe}_{1-x}\text{Co}_x)_{14}\text{B}$ phase. However at additions of over 15 at % there is a reduction in the coercivity of the NdFeB, which has the effect of reducing the Curie temperature. There is also a reduction in the saturation magnetisation that is associated with the substitution of Fe. A secondary effect of Co additions is that there is an improvement in corrosion resistance even with small additions of Co. This is due to the Nd rich grain boundary phase forming Nd_3Co or $\text{Nd}(\text{Fe},\text{Co})_2$ which is less reactive than Nd (Kim,1996).

2.9.3. Copper

The addition of Cu in small amounts to NdFeB can have the effect of improving the coercivity of the material (Pandian, 2002). The main effect of Cu additions is to reduce the grain size, which improves the coercivity. The Cu will also form grain boundary phases of NdCu_2 , NdCu and $\text{Nd}_6\text{Fe}_{13}\text{Cu}$ which also increases the coercivity and improves the corrosion resistance of NdFeB magnets.

When Cu and Co are both added to NdFeB magnets in quantities of 1.2 at% cobalt and 0.2 at% copper, there is a substantial increase in coercivity with the maximum coercivity of (~ 1650 kA/cm) being achieved without a reduction in remanence (B_r). There is also an improvement in temperature stability and corrosion resistance (Kim, 1995). This is due to the formation of $\text{Nd}_{15}\text{Co}_4\text{Cu}$ at the grain boundaries (Williams).

2.9.4. Aluminium

Aluminium additions of up to 10 at % are associated with a significant improvement in coercivity (Pandian, 2002), however this comes at the expense of a reduction in the Curie temperature of 8 K per at % added (Williams, 1994). This is a result of an improved Nd-rich grain boundary phase distribution as the Al forms $\text{Nd}_{36}\text{Fe}_{58}\text{Al}_6$ at the grain boundaries (Knoch, 1989). Al is liquid at the sintering temperatures and this has the effect of increasing the wettability of the Nd-rich phase. This grants an improved

densification and ensures a fine grain size distribution (Tenaud, 1991).

Al can also be combined with Co in order to grant extra improvements in coercivity. This improvement is greater than can be observed with either alloying addition independently.

2.9.5. Niobium

Small additions of Nb, as little as 0.5 at %, are used in NdFeB magnets to bring about improvements in coercivity (Pandian, 2002) as shown in Figure 11. This Nb is usually substituted for Fe in the $\text{Nd}_2\text{Fe}_{14}\text{B}$ matrix grains.

A further effect of Nb is that it can reduce the Fe precipitates that form in NdFeB cast alloys. Fe-precipitates can cause problems when crushing the ingots and powder milling and have an impact on the magnetic properties and corrosion resistance. Nb has been found to reduce the levels of precipitated Fe by 50%, which therefore reduces the annealing time that is required in order to remove it (Liu, 1992).

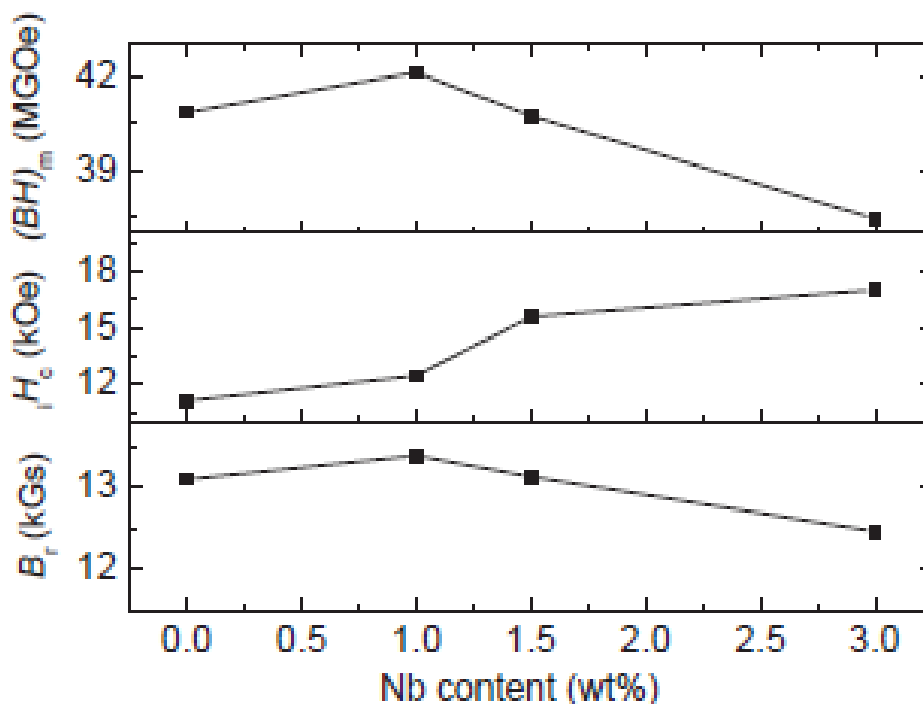


Figure 11 -Effect of Nb content on the magnetic properties of NdFeB. It can be observed that there is an increase in coercivity, an increase in BH_{\max} with up to 1 wt % Nb content and a slight reduction in remanence. (Yu, 2004).

2.10. Recycling of NdFeB

Sintered NdFeB magnets have a similar microstructure to the cast NdFeB alloys, however, the grain size is approximately an order of magnitude smaller (Cast approximately 100-200 μm , sintered approximately 5-10 μm). Sintered magnets react with H_2 in a similar fashion to the cast material (Figure 12); Breaking up into a hydrided form of the powder. Workers in the Magnetic Materials Group at The University of Birmingham have been using this effect to separate NdFeB magnets from electronics.

NdFeB magnets are the most readily decrepitated of all the magnetic materials with hydrogen decrepitation occurring at hydrogen pressures as low as 1 bar and at room temperature (Harris, 1987).

This hydrogen decrepitation can be affected by a number of factors and these can act to speed up, slow down or can even stop hydrogen decrepitation from occurring entirely. The first factor is the oxide layer that forms on the surface of the NdFeB magnet. This oxide layer can act as a barrier to hydrogen as it slows the diffusion of the hydrogen through the surface of the material. Once the hydrogen decrepitation reaction begins however, fresh material will be exposed to the hydrogen and the reaction will become self-accelerating. This effect can also be seen when the surface of the material is contaminated. Other factors that can affect the hydrogen decrepitation are the mobility of the hydrogen within the system and the pressure and temperature of the reaction environment.

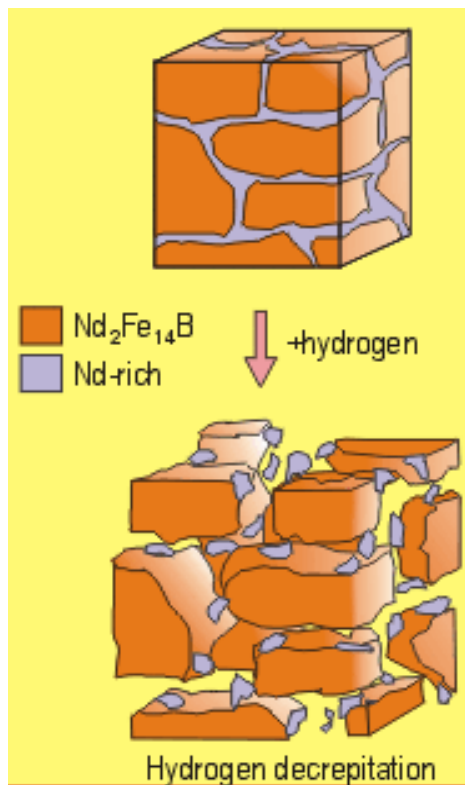


Figure 12 - Schematic of hydrogen decrepitation.

Walton et al [2012] used hydrogen gas to separate the NdFeB magnets from scrap hard disk drives. The hard disk drives were pre cut prior to hydrogen processing using an industrial cropper and pressed using a uniaxial press to distort the magnets. The hard disk drives were then exposed to hydrogen at 2 bars for 2-4 hours to hydrogen decrepitate the NdFeB magnet contained in the voice coil assembly. Crucially the hydriding process demagnetises the NdFeB material so it can be easily separated from other components. The extraction rate of the NdFeB voice coil magnet was estimated to be around 90%. After exposure to hydrogen, the hard disk drives were placed into a rotating porous drum, which was rotated for 50 minutes at approximately 60rpm. This caused the demagnetized decrepitated NdFeB powder to fall through the holes in the drum into a collection vessel which could be sealed in argon. The separated material then contained Ni coating flakes from the magnets and small electronic components. By sieving it was possible to reduce the Ni contamination down to approximately 300ppm as the sieving rate of the Ni is different than the NdFeB powder.

Walton et al, 2012 outlined several possible reprocessing routes for the separated hydrided powders (Figure 13):

1. A refining processing could be used to separate the Rare Earth elements from the NdFeB alloy. The alloy would only contain 2-3 rare earth alloys as opposed to 10 in a primary ore; it would also not contain any radioactive material. However, a lot of energy and cost would be associated with this route as the elements would then have to go back through the same magnet manufacturing route as the primary material.
2. It may be possible to re-cast the powders back into master alloys, but no research has been published in this area to date.
3. It is possible to re-sinter the separated hydrided NdFeB back into new magnets as shown by Zakotnik et al, 2010.
4. It is possible to produce material suitable for resin-bonded magnets. Sheridan et al, 2012 have shown that by using the HDDR route it is possible to produce anisotropic material which would be suitable for commercially viable resin bonded magnets.

Zakotnik et al [2010] hydrogen decrepitated and milled NdFeB magnets before aligning, pressing and sintering to produce new magnets. The author found that upon subsequent re-processing of these magnets there was a progressive fall in the magnetic properties of the magnets. This was due to the oxidation of the magnets during re-processing. Further studies were completed with 1at.% neodymium hydride added each time the magnet was reprocessed. The results displayed that the magnetic properties of the magnets were maintained up to and including the 4th cycle of hydrogen re-processing.

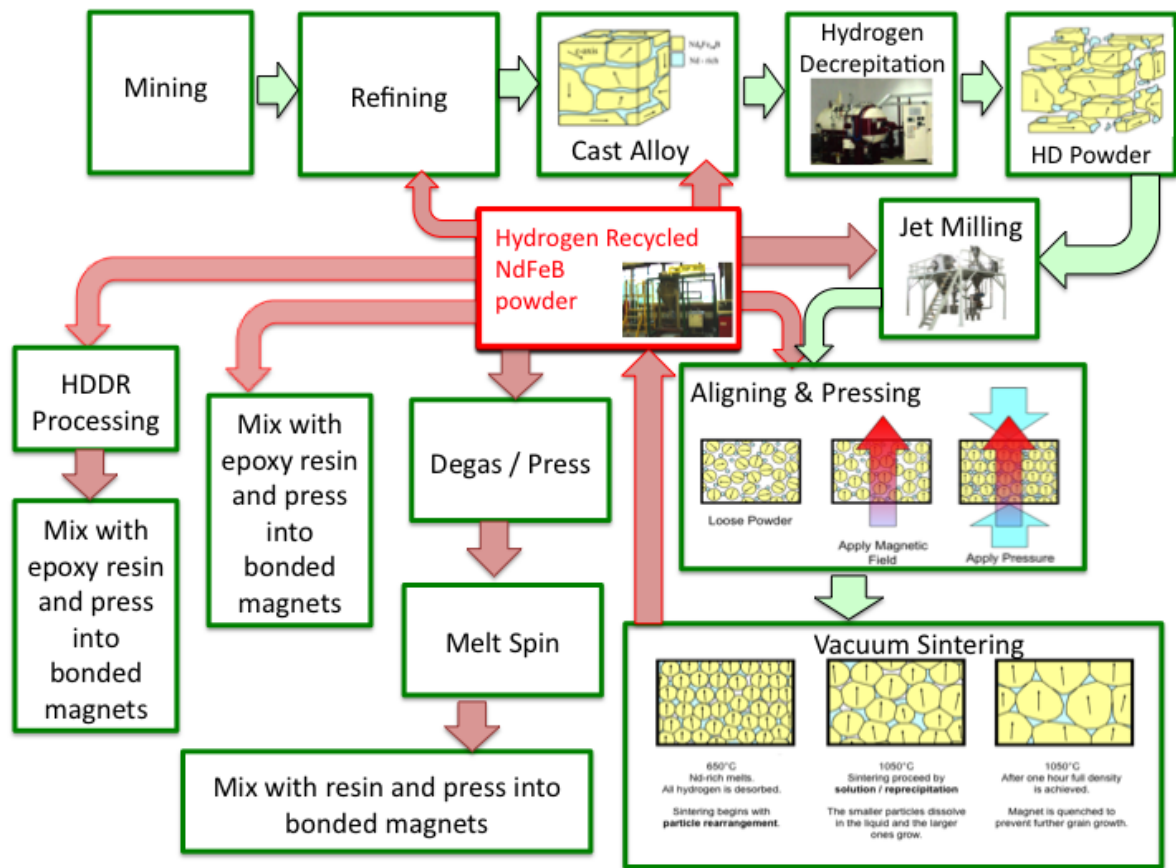


Figure 13 – Production and recycling route for NdFeB voice coil magnets for hard disk drives. Walton et al [2012].

3. Aims

To date the hydrogen separation technique has only been applied to hard disk drive magnets which have a fairly narrow range of composition and low Dy content. The aim of this project was to investigate whether this technology could be applied to other forms of scrap including large rotors from electric vehicles. The magnets used in these applications are typically very different in composition (high Dy content), they are glued onto a large shaft (which presents problems when trying to break the magnets for activation), they are typically uncoated (unlike HDD magnets) and as such they are more likely to have a considerable surface oxide.

This MRes project is to the author's knowledge the first preliminary study of hydrogen interactions on large rotor assemblies. The aims of this project were as follows:

- To investigate whether the HD process can be used to remove magnets completely or selectively from large rotor assemblies.
- To investigate various coating materials to act as masking agents to prevent hydrogen decrepitation.
- To investigate the thermal and mechanical impact on the underlying substrate during hydrogen decrepitation.
- No earlier work has examined the nucleation and growth of oxides on solid/sintered NdFeB surfaces at room temperature. The present work aims to investigate the initiation and early stages of growth of oxides on NdFeB surfaces in air at room temperature.
- Investigate the effect of creating surface damage to the NdFeB magnet on the initiation of hydrogen decrepitation.

4. Experimental Procedure

4.1. Starting materials

Hard drive magnets from Phillips in Southport (now shut down) were used as the starting material. The composition of the magnet material was $\text{Nd}_{14}\text{Dy}_{0.6}\text{B}_6\text{Al}_{0.7}\text{Fe}_{78}\text{Nb}_{0.4}$. NdFeB magnets were stripped of their protective Ni coatings by grinding with P120 silicon carbide grinding paper. The magnets were then allowed to oxidize at room temperature for one week. This composition of sample was used for the coating, confocal, Raman and strain experiments.

4.2. Hydrogen Processing

Two pressure vessels were used in order to process sintered NdFeB magnets in hydrogen. The pressure vessels were evacuated using a rotary vacuum pump to 10^{-2} mBar and then back filled to 2 bar absolute, the hydrogen purity was 99.9%.

4.3. Coating Experiments

Three masking agents were used to coat NdFeB magnets. These included; nail varnish a), Gestetner lithographic correction fluid b) and Tetra Ethyl Ortho Silicate (TEOS) c). The coatings were applied once with a brush to a thickness where the samples were completely covered in the coating.

4.4. Commercial Assembly Experiments.

Medium to large rotor assemblies from electric vehicles (including the electric smart car) were provided by Arnold Magnetics (Figure 14). These were used to test the effects of hydrogen decrepitation on commercial assemblies. The composition of these magnets is presently unknown. The magnets were of a high grade and therefore are likely to contain high levels of Dy. The Dy levels in electric motors are commonly observed to be around 6-8%.

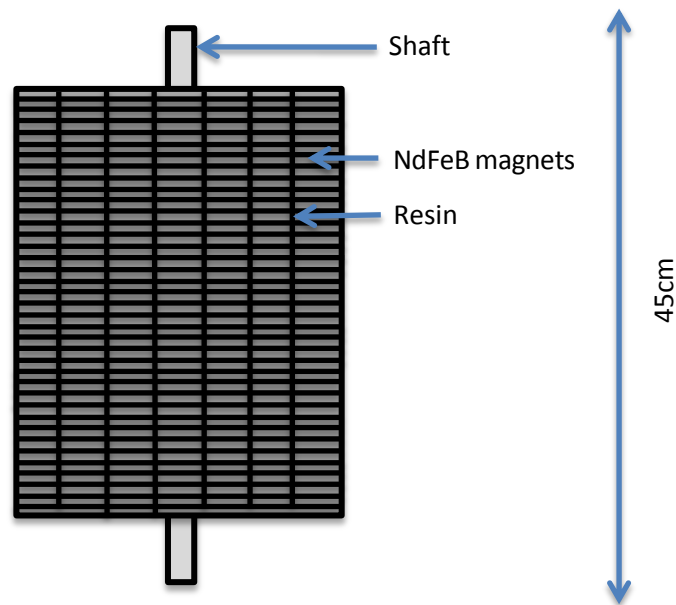


Figure 14 - Schematic diagram of the commercial rotor assembly from a Smart car. Each individual magnet was approximately 1cm x 4cm.

4.5. Flat Plate Assembly

A flat plate assembly was made in order to simulate a commercial array of magnets in a simpler configuration. The assembly consisted of a steel base plate that held nine uncoated NdFeB magnets of the same composition as the HDD magnets. These magnets were glued onto the base plate using Araldite epoxy resin. Some of the magnets were coated (as described above) in order to prevent hydrogen decrepitation.

Low Voltage Temperature Sensors (manufactured by Analog Devices) were used to measure temperature changes during hydrogen decrepitation. The temperature sensors had a $\pm 2^\circ\text{C}$ accuracy and could operate between -40°C to $+125^\circ\text{C}$. The temperature sensors were attached to the assembly using a small amount of resin on the underside of the temperature sensor. They were positioned with one on the resin between the central magnet and an outer magnet, in the centre of an outer magnet and on the underside of the assembly on the stainless steel plate. The temperature sensors logged to an Arduino Data Logger which was placed in the pressure vessel and recorded versus time. The recording system and software were developed during the course of this project.



Figure 15 - Mock Flat plate assembly before hydrogen exposure with temperature sensors attached.

4.6. MagScan

A Redcliffe MagScan was used to measure the magnetic field of the flat plate assembly before and after hydrogen decrepitation. This information was used to evaluate the damage created to magnets in the assembly. The MagScan consists of a Hall probe which can be moved in a pre-programmed area using a series of motors. The resolution setting used in this project was 1mm x 1mm over an area of 300mmx300mm.

4.7. Microscopy

The samples used for scanning electron microscopy and confocal microscopy were prepared by mounting the sample in bakelite and grinding to a P1200 finish using silicon carbide grinding paper. The samples

were then polished to a finish of 0.25 μ m using polishing cloths and diamond-polishing paste.

For the work on the oxide layer of the NdFeB magnets, scrap, magnets that had been exposed to the atmosphere for a considerable amount of time (>1 year) were used to provide an example of a worst case scenario. NdFeB magnets from Ugimag, China were used with a composition of Nd_{12.52}Pr_{0.17}Dy_{1.8}Fe_{72.49}B_{6.44}Al_{0.88}Co_{4.98}Nb_{0.61} at% which had been found previously using ICP analysis done by Less Common Metals Ltd. However, this led to problems in how the samples were mounted before SEM imaging. The oxide layer, which had built up on the surface of the magnet, was very brittle and therefore when it was mounted using conventional mounting processes such as a Bakelite press, the oxide layer was damaged and broke away from the magnet.

In order to solve this problem vacuum impregnation was used to protect the oxide layer. Furthermore, a secondary resin ring was added to the outside of the vacuum impregnated resin. This layer was harder than the first layer, allowing the sample to be ground and polished flat.

A Jeol 7000 SEM equipped with Wavelength dispersive X-ray spectroscopy was used to image the sample and measure the occurrence of oxygen within the sample

An Olympus Lext OLS3100 confocal laser 3D microscope was used to assess the initial stages of oxidation on the NdFeB magnets. In order to activate the surface of the NdFeB magnets they often have to be scratched using a scalpel. The confocal microscope was used to assess the depth of any surface activation on the surface of the magnets after scoring with a scapel or a Maplins N48FT Dremel tool.

4.8. Raman Spectroscopy

A Renishaw inVia raman microscope was used in order to identify the composition of the oxidation corrosion products developed in air on the surface of the NdFeB magnets. 3D images were taken of NdFeB magnets at 20-second intervals in air up to 360 minutes. Depth profiles were produced to calculate the highest point on each triple point with time. The magnet was first ground and polished

using the procedure explained above. It was then exposed to air at room temperature for 3 hours in order to allow the sample to oxidise.

4.9. Encapsulation Experiments.

In order to attempt to measure the strain developed as a result of encapsulated NdFeB magnets decrepitation the magnets were cut into discs that were 3mm in diameter and 2mm in depth using erosion cutting. Copper tubes with an inner diameter of 3mm and an outer diameter of 4mm were fitted around the magnets, as shown in

Figure 16. The magnets were then ground and polished before being scored with a scalpel and exposed to hydrogen at 2 bars for 2-4 hours. An Olympus LEXT OLS310 Confocal Scanning Laser microscope and a micrometer were used to measure the dimensions of the copper after hydrogen decrepitation.

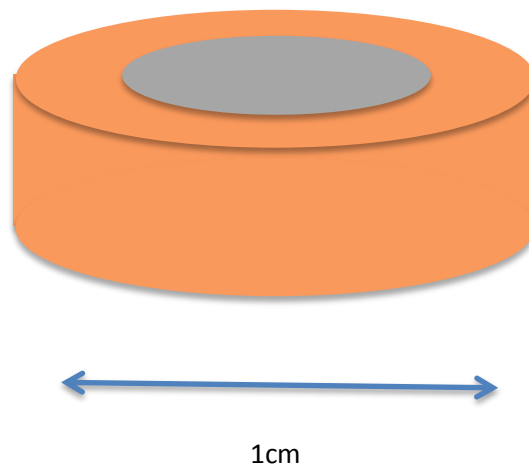


Figure 16 – Schematic diagram of the NdFeB magnet encapsulated in a Cu ring.

5. Results and Discussion

5.1. Selective Removal of NdFeB Magnets

5.1.1. Coating Experiments.

Three barrier layers were applied to NdFeB magnets using a brush; nail varnish a), Gestetner lithographic correction fluid b) Tetra ethyl ortho silicate (TEOS) c). A fourth set of magnets were left uncoated d).

Nail varnish was chosen as it can easily be dissolved in acetone once the decrepitation experiments had been completed. Gestetner lithographic correction fluid was chosen as it is already used as a masking agent in lithography and tetra ethyl ortho silicate (TEOS) was chosen as it has previously been shown by another member of the group to demonstrate resistance to hydrogen when used to coat bonded magnet powders.

The first experiments involved the exposure of coated and uncoated NdFeB magnets to 2 bars of hydrogen for a total of 3 hours; the samples were monitored throughout the 3 hours and photographed. Decrepitation of the TEOS coated magnets and the uncoated samples were observed after around 15 minutes. After one hour the samples which had been coated in TEOS were partially decrepitated, with only one half of one of the samples being undamaged. The uncoated samples had completely decrepitated to form granules and powder. After a further two hours, the samples were removed and photographed (shown in Figure 17). There was no discernible damage to either the sample coated in nail

varnish or Gestetner lithographic correction fluid. The particle size of the other two samples appeared to have been reduced further.

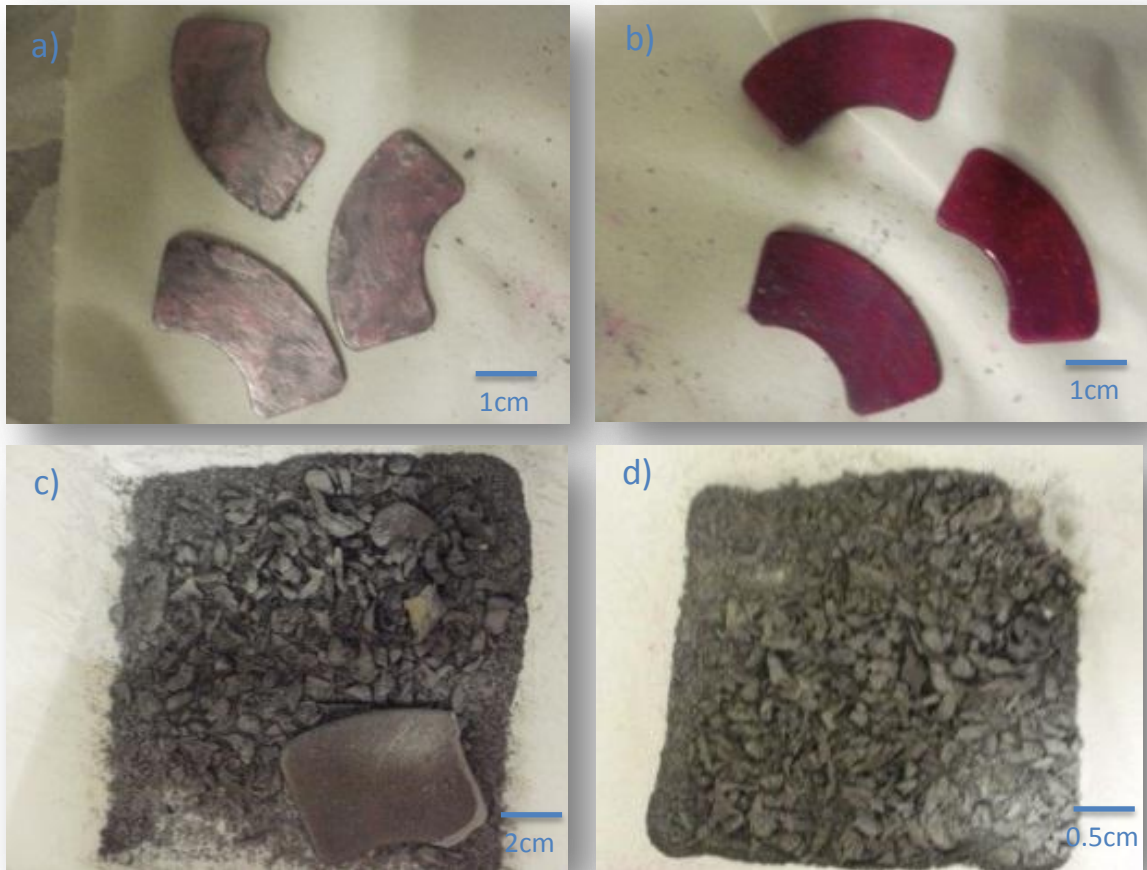


Figure 17 - Voice coil magnets coated in a) Nail Varnish b) Lithographic Correction Fluid c) TEOS d) uncoated.

This investigation demonstrated that a magnet could be protected successfully from hydrogen decrepitation, under the specified conditions, by the application of a barrier coating as simple as nail varnish. It is very unlikely that hydrogen does not diffuse through this coating, given the size of the hydrogen molecule. This barrier coating is likely to simply slow the diffusion rate of hydrogen to the surface. In the time required to decrepitate the other magnets in an assembly this would provide sufficient protection.

The experiments also showed that the oxide layer developed over one week of air exposure after the Ni is peeled away is not sufficient to prevent hydrogen decrepitation for this particular magnet composition.

The TEOS coating was only successful at protecting one half of one magnet, which shows it has limited potential as a protective coating. This coating is also the most difficult to handle and apply as it is highly volatile. Due to the high volatility of this substance, it may be that it needs to be applied and dried in a more controlled manner and it may need several coatings in order to be as effective as some of the other coatings such as the nail varnish.

Due to the effectiveness of the nail varnish at protecting the magnets against hydrogen decrepitation and the fact that it can be removed easily by acetone post H₂ treatment, it would seem that this is the most likely candidate as a barrier coating. It is also easy to apply to small batches and could be simply scaled up by using techniques such as spraying. This would give a greater control over the thickness of the coating and the surface finish and would increase the application speed if large sections of magnet needed to be coated.

Previous unpublished work by Allan Walton in the University of Birmingham Magnetic Materials Group demonstrated that by attaching pressure cells to the resins surrounding NdFeB magnets in assemblies it was possible to selectively remove some of the magnets using hydrogen processing. In this project, barrier layers were investigated to mask selected NdFeB magnets and then the whole assembly was placed in hydrogen.

5.2. Commercial Assemblies.

A commercial rotor assembly from a Smart Car provided by Arnold Magnetics Ltd was subsequently used for the masking experiments. Half the magnets were painted with nail varnish to protect them against hydrogen decrepitation. The whole assembly was then exposed to hydrogen. After exposure to H₂ at two bar pressure for two hours, the sample was then removed and photographed. After two hours, none of the magnets in the assembly had reacted with hydrogen. The magnets mounted onto this rotor will

have been exposed to air for a considerable length of time (> 6 months). It is likely that the surface oxide has built up to such a degree that hydrogen decrepitation is slowed and therefore needs to be broken to expose fresh material to hydrogen in order for hydrogen decrepitation to initiate.

Therefore, half of the uncoated magnets that had not reacted initially in hydrogen were then scored and the assembly was re-inserted into the vessel and exposed to hydrogen for a further two hours after the masking agent was removed. Upon removal of the rotors it was shown that all of scored magnets had been fully decrepitated and the surface of the steel base was left clean with a small amount of brittle, compacted magnet powder remaining on the surface, this powder could be brushed off easily. The unscored magnets were then scored and placed back into the vessel. After a further two hours the assembly was removed and it was observed that the remaining magnets had been decrepitated. There was no evidence of any initial dimensional change to the underlying rotor or to the surface of the rotor and it is likely that the shaft of the rotor could easily be re-used and fitted with new magnets.

When the assembly was removed from the vessel, it was revealed that it had been made up of three separate parts, which had been held together by the attraction of the magnets and a small amount of resin. Upon decrepitation, the three parts had separated. Subsequently tests were performed after this experiment on an identical assembly to try to split it into three parts by alternative methods. The assembly was mounted in a three-point bend test. Two tonnes of force was exerted on two sections of the magnet assembly yet it remained intact. This provides an interesting example of the amount of force which is developed by the hydrogen decrepitation process.

This experiment has demonstrated that scoring the magnets is a useful way of initiating hydrogen decrepitation on the surface of the NdFeB magnets. In this experiment a scalpel was used to scratch the magnets, however, as this is done by hand, there is significant variability in the depth of the score. It would be useful to understand the minimum depth of score required in order to break through a typical surface oxide on an NdFeB magnet. An attempt was made during this project to characterise the depth

of the oxide layer and the depth of the score using SEM and confocal laser microscopy.

NdFeB section



Un-scored magnets

Scored magnets



Resin left on the surface
of the assembly.

Figure 18 - Photographs of the commercial assembly a) before b) Half the magnets were scored and half were left un-scored c) after hydrogen decrepitation

5.3. Oxidation Experiments

5.3.1. SEM imaging

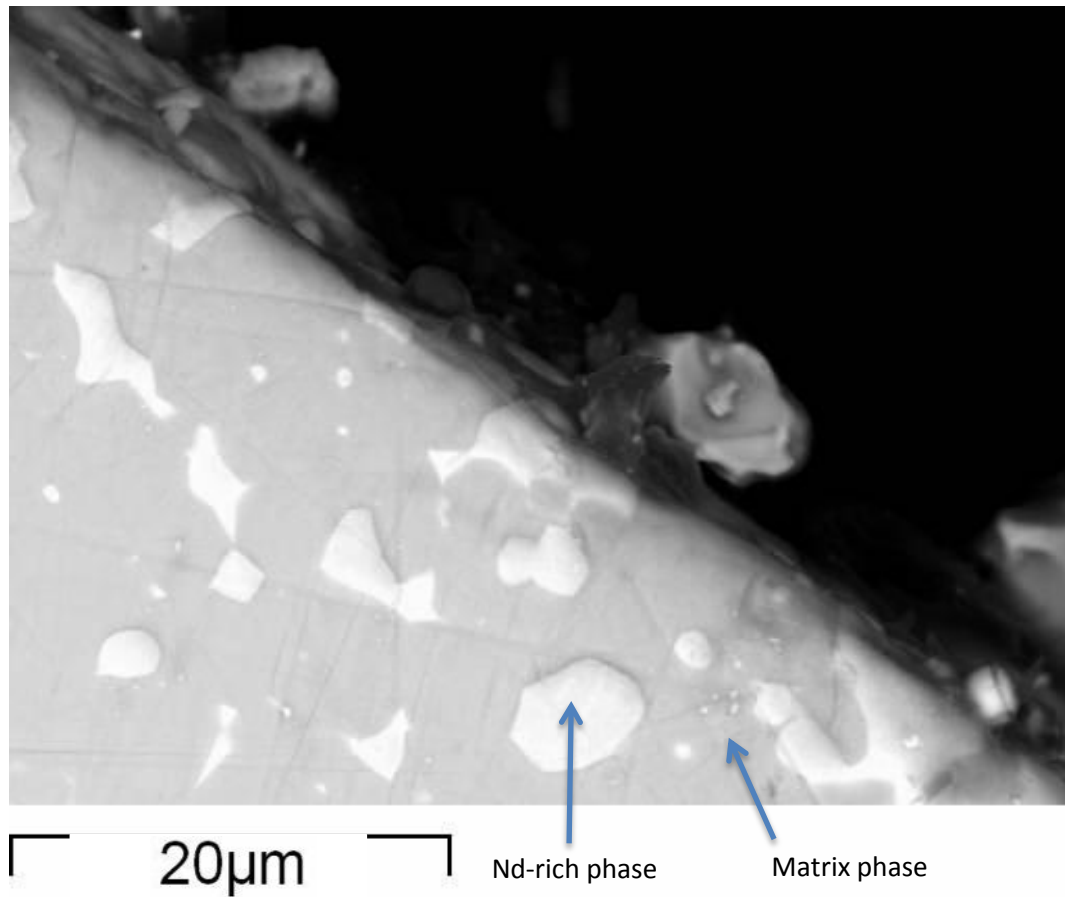


Figure 19 - Backscattered SEM image of NdFeB magnet.

It was evident from the hydrogen decrepitation studies on NdFeB magnets that the surface condition of the magnets plays a key role in the initiation of hydrogen decrepitation. For this reason SEM analysis was performed to assess the surface region of the scrap magnets.

5.3.2. SEM with EDS

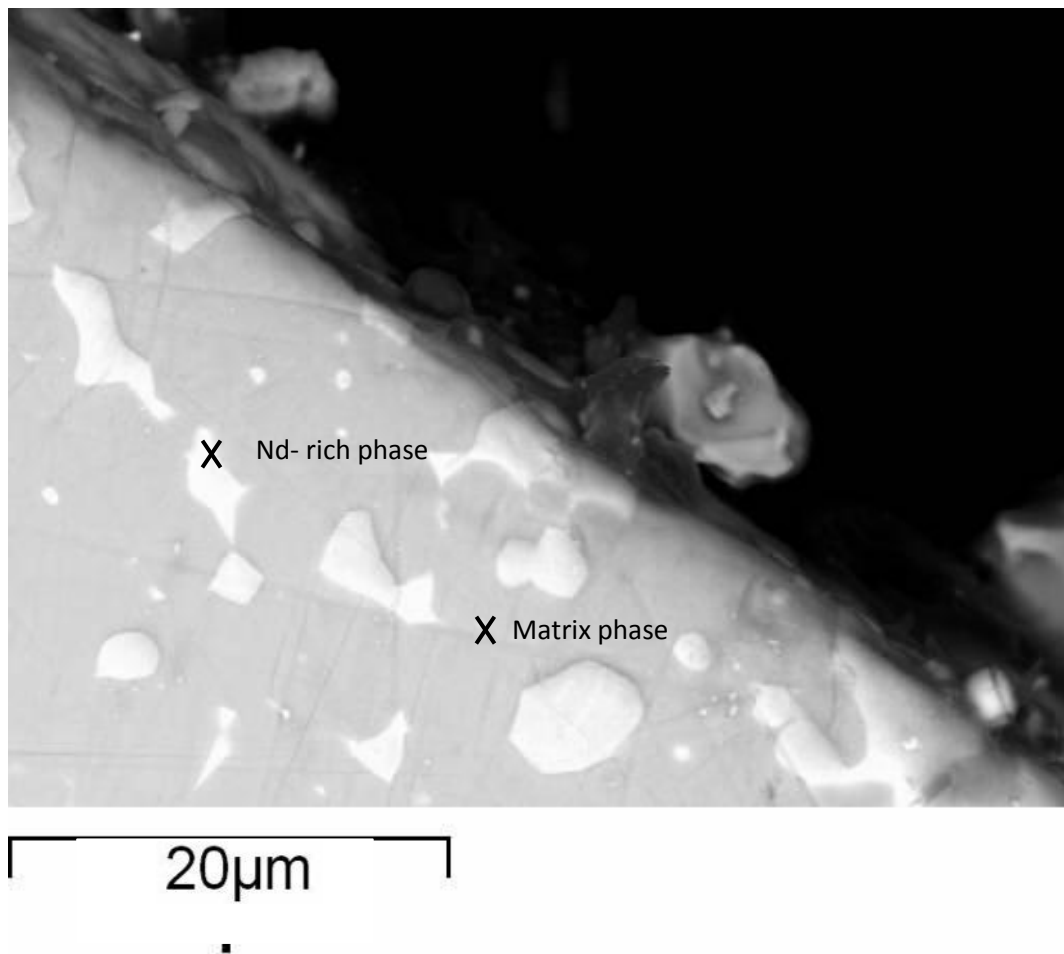


Figure 20 - Backscattered SEM image of NdFeB magnet with a composition of $\text{Nd}_{12.52}\text{Pr}_{0.17}\text{Dy}_{1.8}\text{Fe}_{72.49}\text{B}_{6.44}\text{Al}_{0.88}\text{Co}_{4.98}\text{Nb}_{0.61}$ at%, which had been exposed to air for over 1 year. The image clearly shows the Nd-rich grain boundary phase that has pooled during sintering at the triple points, surrounded by the $\text{Nd}_2\text{Fe}_{14}\text{B}$ grains. EDS analysis shown in Figure 21 and Figure 22 confirmed the phases.

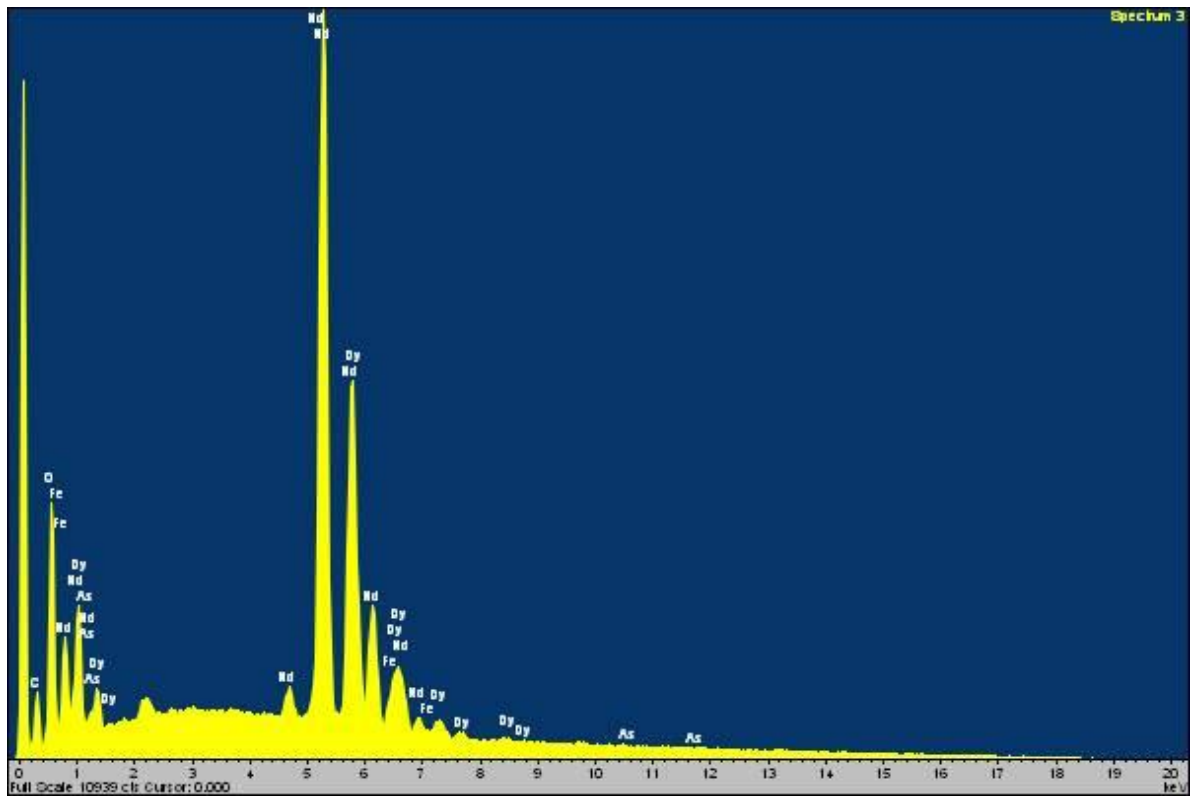


Figure 21 - EDS spectrum for the Nd rich phase in NdFeB magnet displaying that the spot mainly consisted of neodymium.

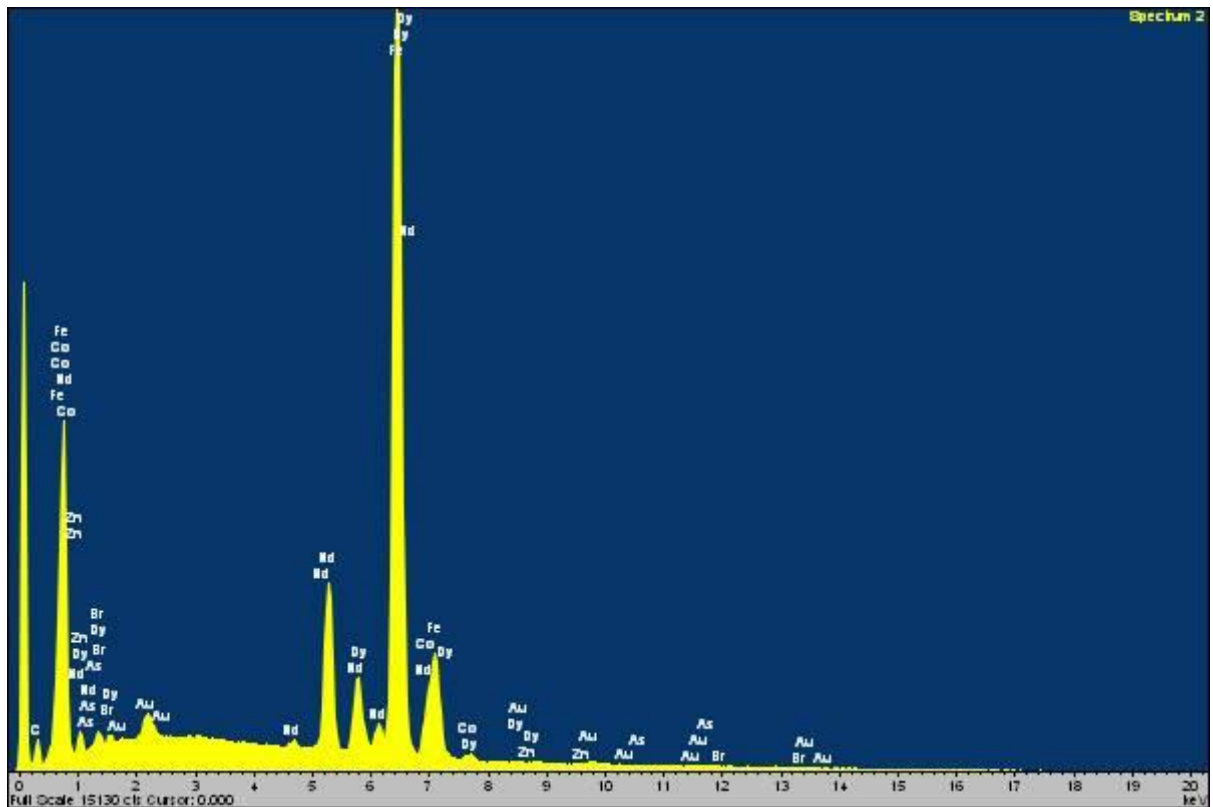


Figure 22 - EDS spectrum for matrix phase of NdFeB magnet displaying that the spot over the matrix phase consisted of mainly iron with a smaller amount of neodymium.

5.3.3. SEM with WDS

In order to obtain an accurate reading of the oxygen content in the NdFeB magnet, wave dispersive spectroscopy was used. A WDS line scan was performed from the edge of the sample at a triple point moving into the sample. The results of this experiment are displayed in Figure 24.

This data shows that there is an oxide layer that is around 3 μ m thick; concentrated in the Nd- rich grain boundary triple point, which was identified by E.D.S earlier in this project. The matrix phase is displayed between 3 and 10 μ m. This has an oxygen content of around 0.5 at%.

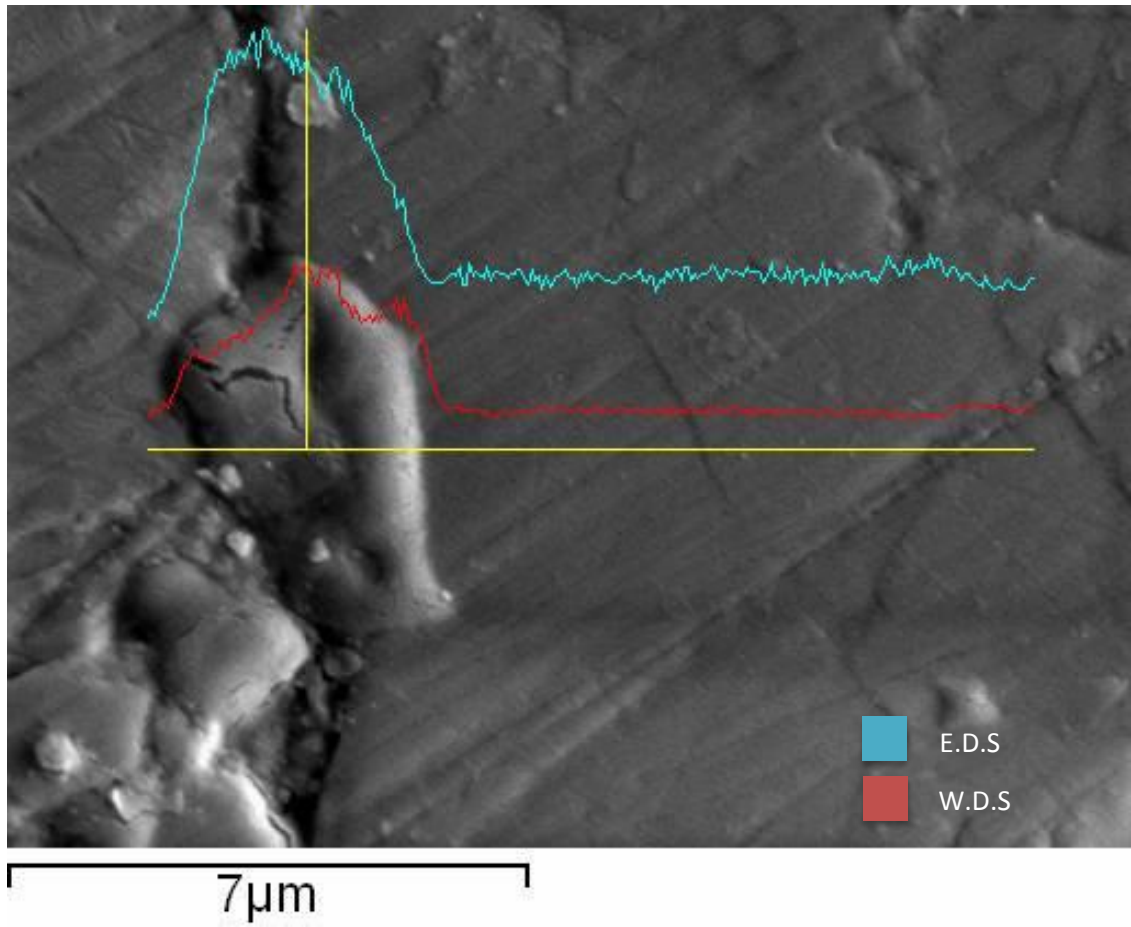


Figure 23 - W.D.S and E.D.S line scan of the oxygen content in an NdFeB magnet.

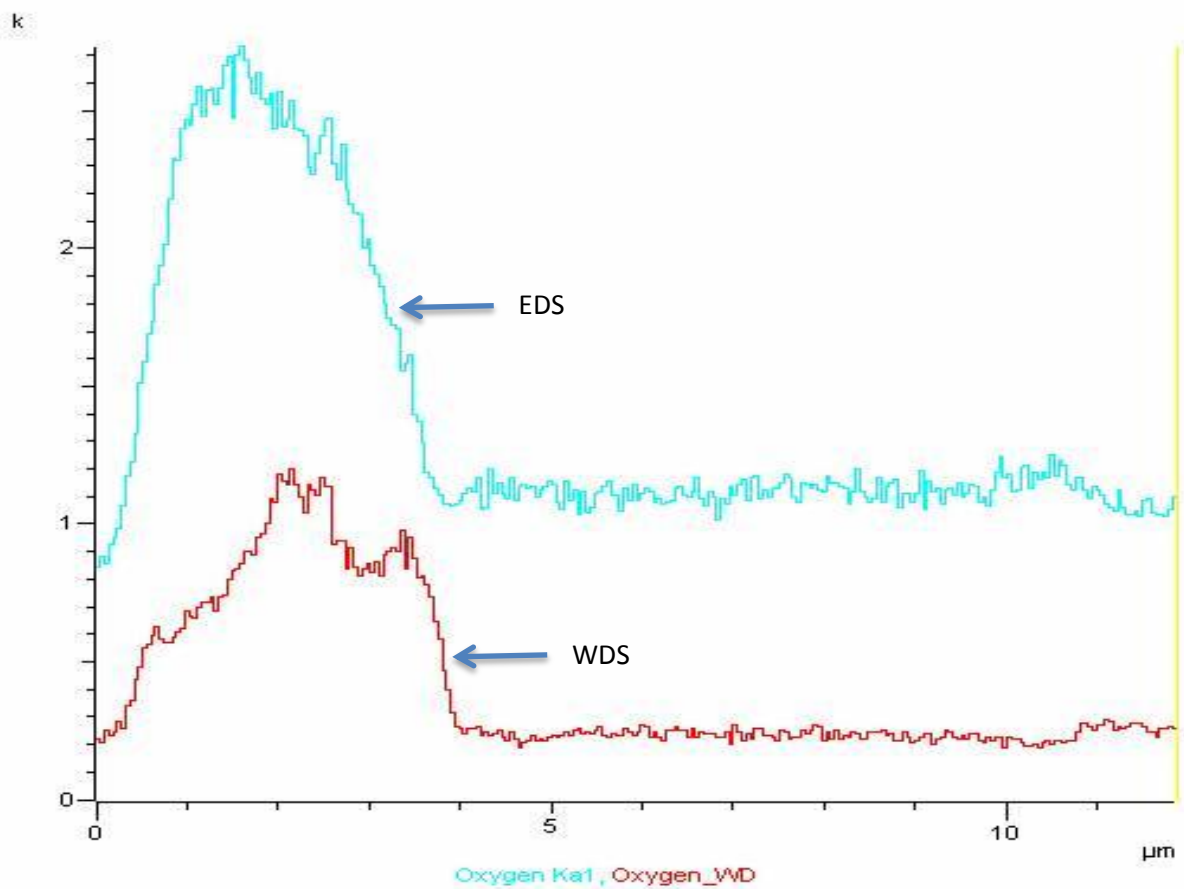


Figure 24 - W.D.S and E.D.S line scan of oxygen content in an NdFeB magnet.

5.3.4. Confocal Microscope Observations of Oxide Growth Morphology and Kinetics

The SEM cross sectional analysis clearly demonstrated that the triple points in the NdFeB material had oxidised preferentially compared to the matrix phase when exposed to air for prolonged periods of time. There is only a relatively small amount of information in the literature on the oxidation of NdFeB at room temperature in atmospheric conditions and most of these studies have concentrated on NdFeB powders. An attempt was therefore made to use 3D-Confocal Microscopy to track the oxidation behaviour on polished NdFeB surfaces on first exposure to air.

NdFeB samples were polished in an argon glove box, and the samples were exposed to air at room

temperature under the confocal microscope. 3D images were taken at 20-second intervals for a period of 6 hours at 100x magnification, however the height of the triple points was not measured for each of these images, with the images early in the experiment being measured more frequently than later on in the experiment. The 3D images for the first 60 minutes of air exposure are displayed in Figure 25 and Figure 26. It was evident that platelet type structures had nucleated selectively on the exposed NdFeB surface at grain boundary triple points, which EDS has shown to consist of a Nd-rich phase. The platelets began to grow at the edges of the triple points with the centre of each platelet remaining flat. After approximately 50 minutes of air exposure, the centre of the platelets began to grow upwards and eventually became the highest point in the platelet. The variation in the rate of growth of the different areas of the triple point could be due to the varying composition in the triple point, as described in the literature review section of this thesis.

During the current experiments (max-6hours) there was no evidence of a non-uniform increase in the height of the Nd₂Fe₁₄B matrix phase. However the matrix phase could be growing out of the surface uniformly and this would create an error in the height measurement of the grain boundary phase. This is because the matrix phase is used as the reference height in this work.

During the 6 hour exposure to atmospheric conditions at room temperature there was a total average height increase of 0.7µm in the platelets, but no change in the appearance of the matrix phase. Also during this period there was little increase in the lateral dimensions of the platelets.

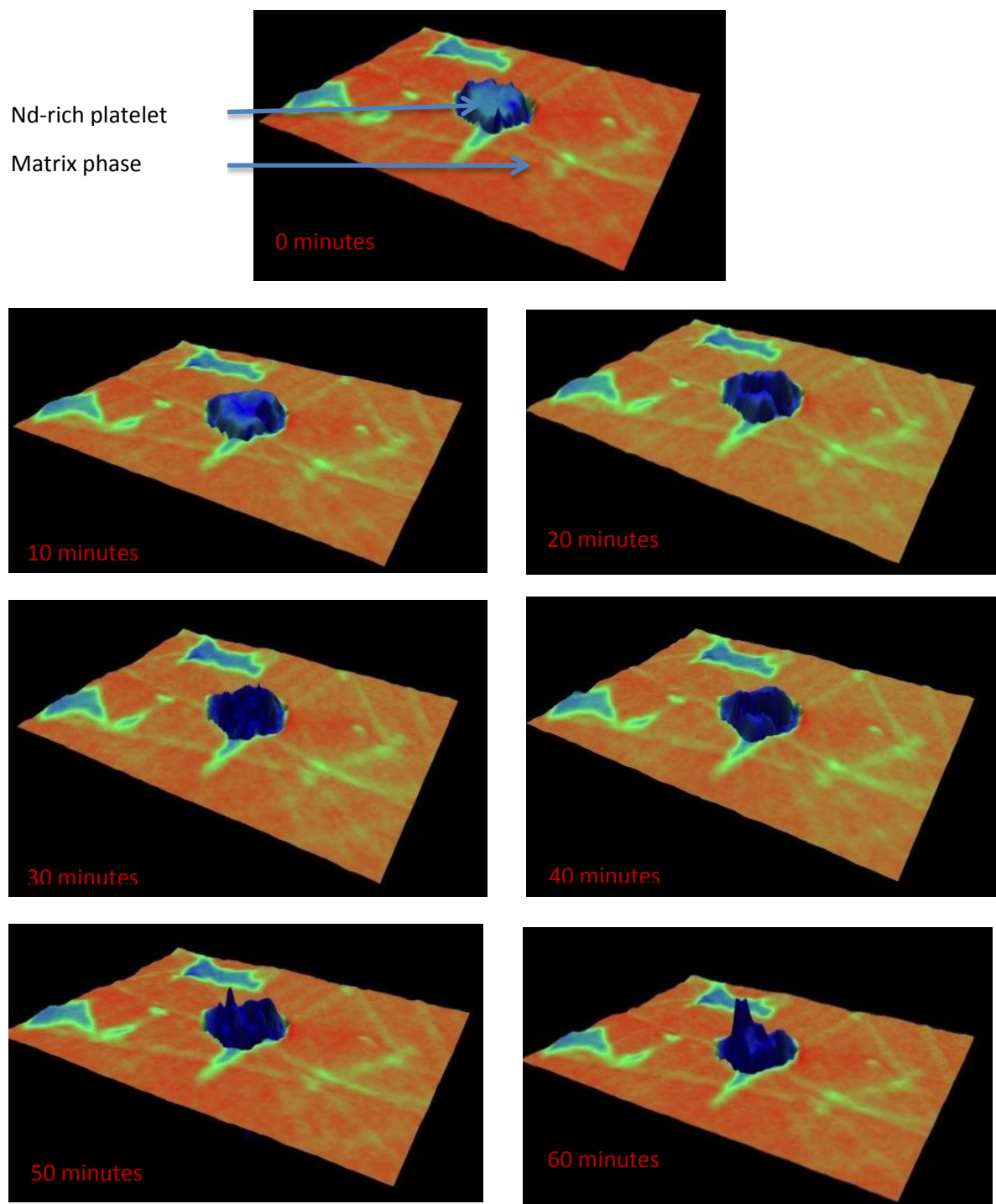


Figure 25 - 3D confocal microscope Images for a Nd rich triple point imaged over 1 hour.

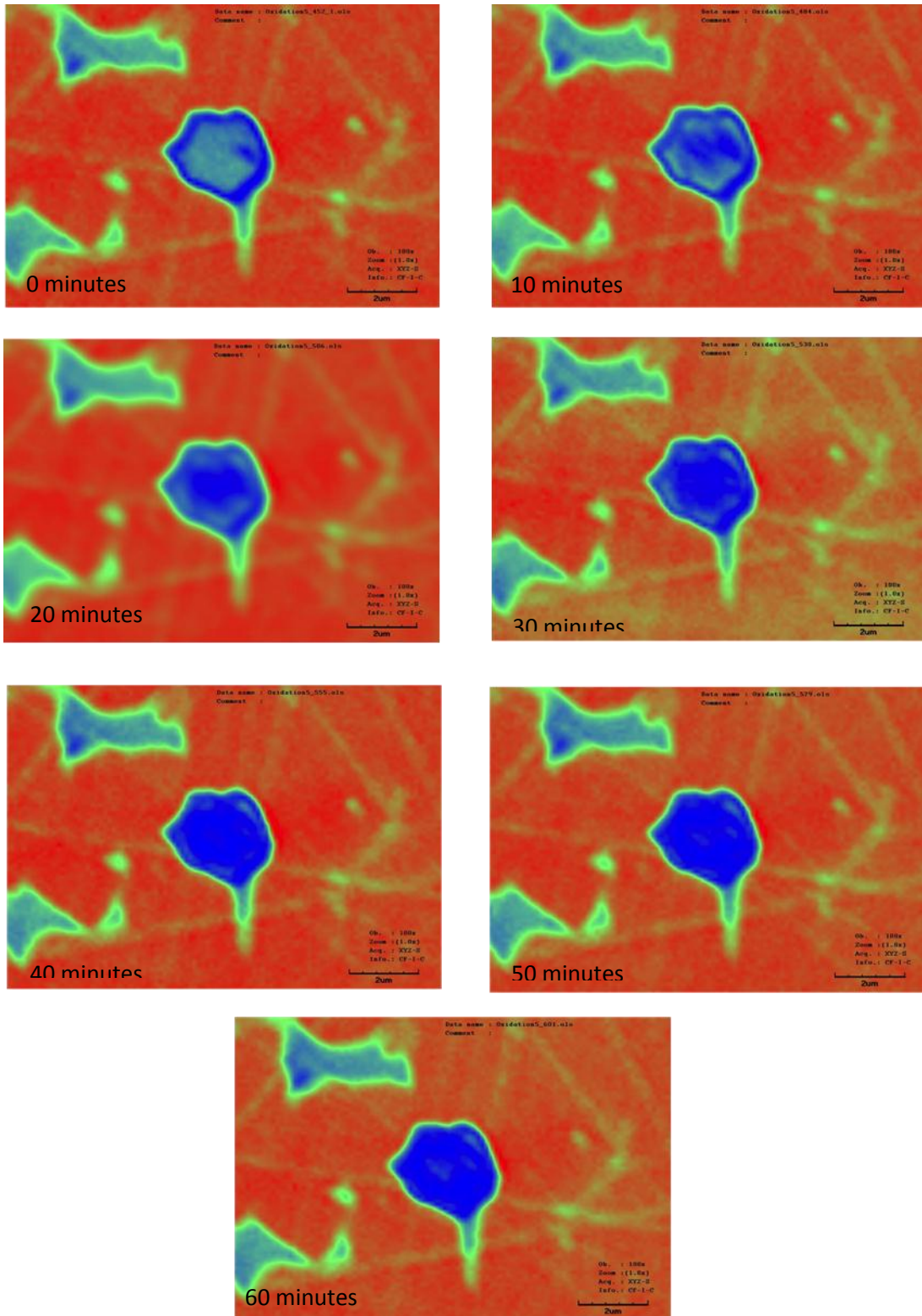


Figure 26 - 2D confocal images of a Nd-rich triple point imaged over 1 hour.

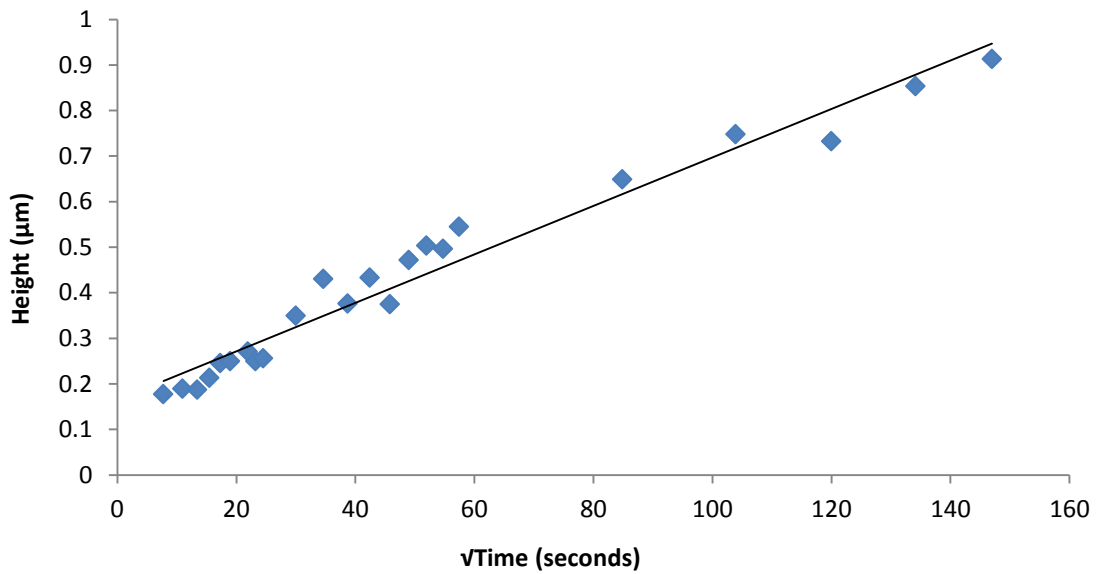


Figure 27 – Height versus the square root of time for 6 Nd-rich triple points in dry and humid air.

When the average maximum platelet height of 6 platelets was plotted against the square root time, a straight line is produced (

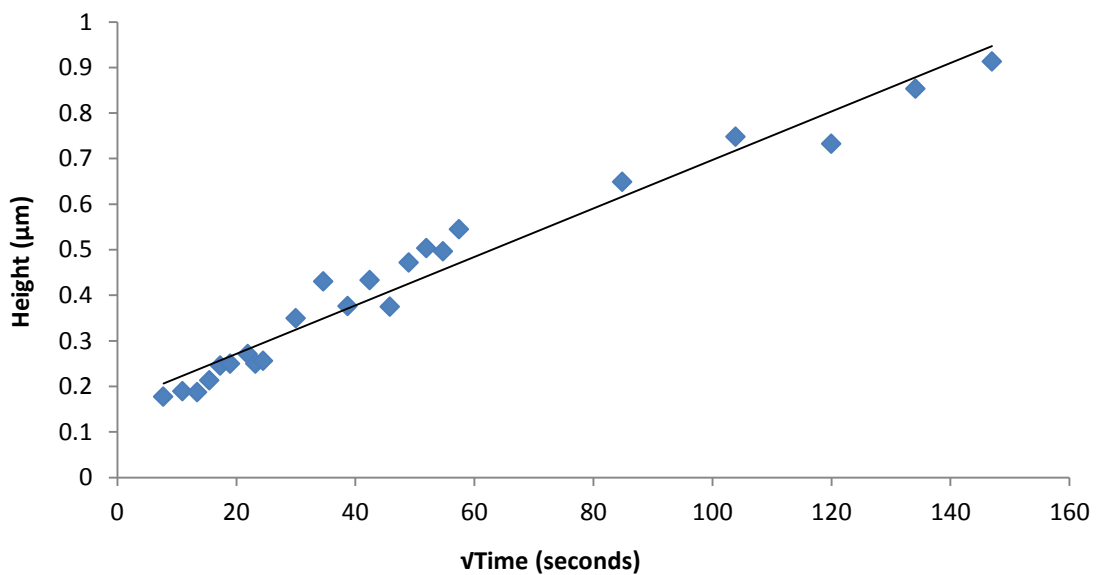


Figure 27). This would suggest that the oxide platelet vertical growth is diffusion controlled. The diffusion coefficient for the growth controlling processes can be calculated by using the formula in

Equation 4, where D represents the diffusion coefficient (cm²/sec), t represents time (secs) and D represents distance(cms).

$$x = \sqrt{Dt} \quad \text{Equation 4}$$

Using this equation a diffusion coefficient of $3 \times 10^{-13} \text{cm}^2/\text{sec}$ [293°K] was calculated. This is similar to the value reported by Wong et al [1990] who calculated a diffusion coefficient of $2 \times 10^{-14} \text{cm}^2/\text{sec}$ for NdFeB in air at 100°C.

The diffusion coefficient observed in the present work is large for a room temperature process, suggesting that the underlying transport mechanism is controlled by grain boundaries and high defect levels, which typically give a diffusion coefficient of approximately this magnitude [Tu et al, 1992]. Further support for this is given by the site and frequency of the oxide platelets. As noted above the oxide platelets are located directly above grain boundary triple points on the NdFeB surface where the local diffusion rates and the concentration of Nd-rich phases are highest.

The confocal microscope is within a laboratory, which has low humidity due to air conditioning. It was observed that when the air conditioning in the laboratory was switched off, there was an increase in the rate of platelet growth of the samples. The increasing temperature in the laboratory may have had an impact on the oxidation rate of the samples. The temperature increased by around 5°C when compared to investigations that were conducted whilst the air conditioning was operational. The diffusion rate for the sample exposed to the non air atmosphere was calculated to be approximately $5 \times 10^{-13} \text{cm}^2/\text{sec}$ (293°K) (

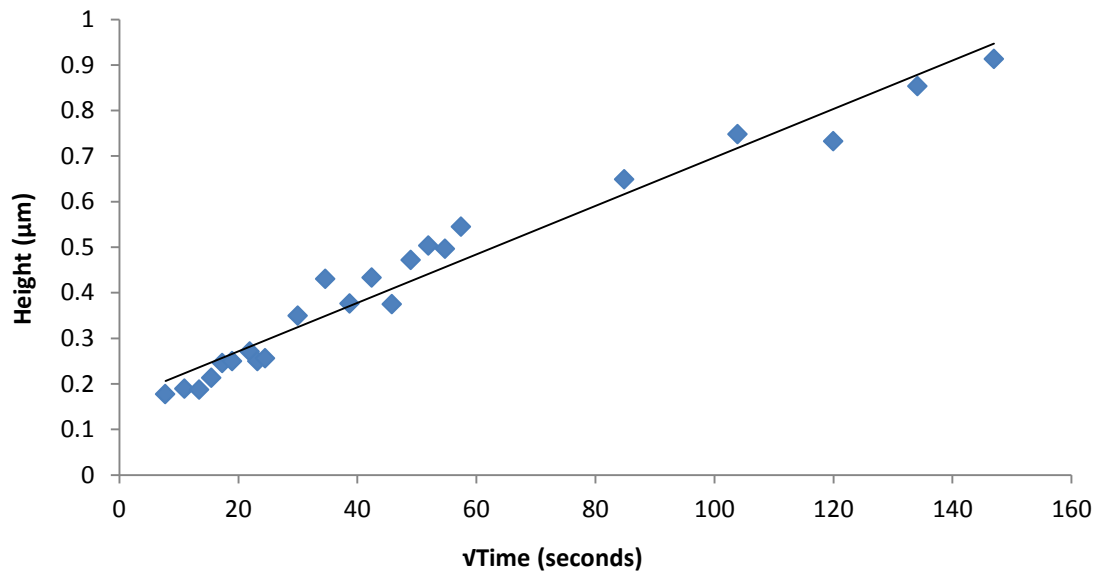


Figure 27).

5.3.5. Raman Spectroscopy

It is known that the Nd-rich phase in NdFeB magnets can form $\text{Nd}(\text{OH})_3$ in humid air at 50-90°C and relative humidity of 50 to 90% (Jacobson and Kim, 1987). Raman Spectroscopy was performed on air exposed samples to identify the oxidation/ corrosion products on the surface of the NdFeB magnets. The NdFeB magnet was mounted in Bakelite and ground and polished in an argon filled glove box. It was then removed from the glove box and allowed to oxidise for a period of 2 hours.

The sample was placed into the Raman Spectrometer and an image was taken by the confocal microscope within the machine. This allowed data to be collected specifically at the triple point.

Strong resonances were observed (Figure 28) in the 100-700 cm^{-1} wavenumber region, which match the spectra that were obtained from an Nd_2O_3 reference specimen. No other peaks were observed which could relate to $\text{Nd}(\text{OH})_3$.

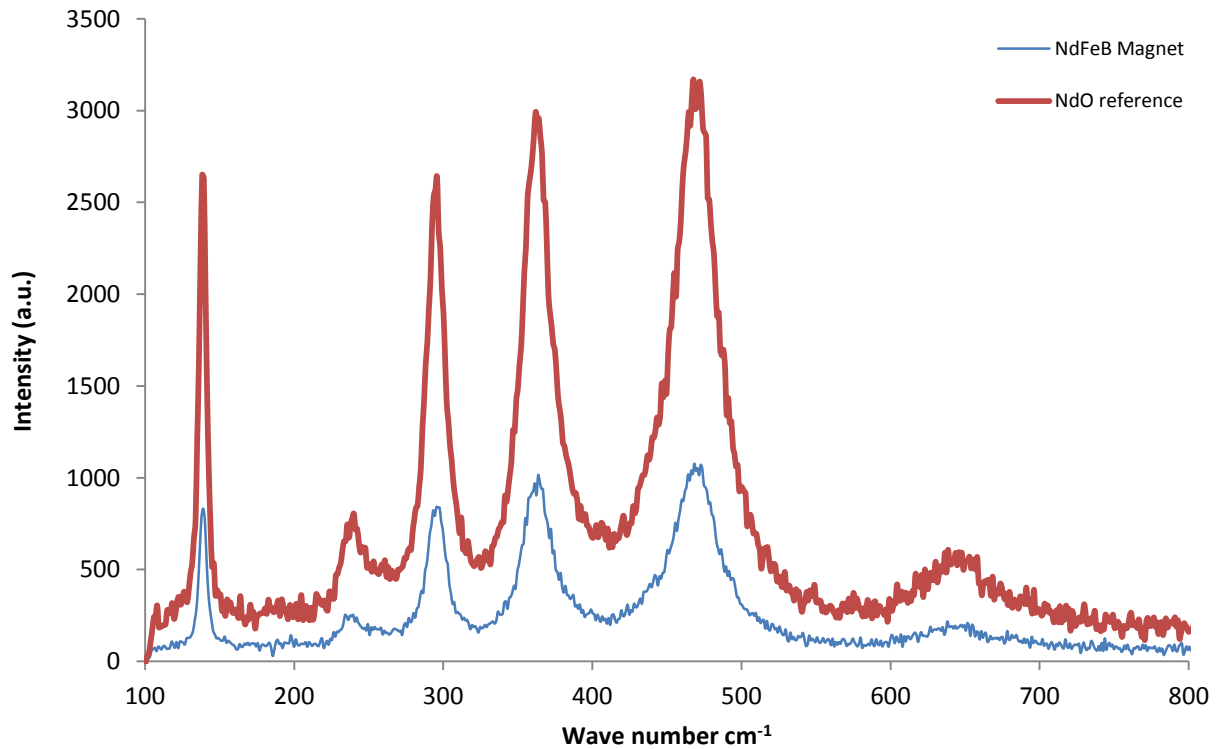


Figure 28 - Raman results for a NdFeB magnet when compared with a Nd_2O_3 reference.

$$D(T) = D_0 \exp\left(\frac{-E_a}{RT}\right) \quad \text{Equation 5}$$

The activation energy for the underlying diffusion process can be derived using the expression in equation 5, providing a value of D_0 (the diffusion constant) is known. Where E_a is the activation energy, R the rare gas constant and T is temperature.

D_0 values for the oxidation of rare earth metals, including Edgley's for Nd (0.01eV) lie in the range

0.01 to 0.001-eV. Using Edgley's [1997] value of D_0 (0.01eV) the activation energy is calculated to be 0.6eV. This activation energy is again typical for defect enforced, surface and grain boundary diffusion. Oxygen migration through the grain boundary phase is likely to be the main mechanism for the growth of the oxide platelets.

No directly comparable low temperature activation energy data for oxidation of NdFeB are available, however, the data from several previous studies of bulk and powdered samples conducted at higher temperatures are given in Table 4 and

Table 5.

Table 4 - High Temperature Oxidation of NdFeB Bulk samples.

| Temperature range (°C) | Atmosphere | Activation Energy (eV) | Reference |
|------------------------|------------|------------------------|-----------|
|------------------------|------------|------------------------|-----------|

| | | | |
|---------|-----|------|------------------|
| 400-600 | Air | 1.22 | Blank, 1987 |
| 360-600 | Air | 0.73 | Lemarchand, 1992 |
| 365-611 | Air | 1.09 | Edgley, 1997 |

Table 5 - Oxidation of NdFeB powdered samples.

| TemperatureRange (°C) | Size(μm) | Atmosphere | Activation energy (eV) | Reference |
|------------------------------|-----------------|-------------------|-------------------------------|------------------|
| 250-276 | <20 | Air | 0.3 | Osawa, 1992 |
| 20-1100 | <20 | Air | 0.4 | Stewart, 1991 |

| | | | | |
|---------|---------|-----|------|------------------|
| 360-600 | 800-100 | Air | 0.44 | Lemarchand, 1992 |
| 100-250 | 4 | Air | 0.25 | Higgins, 1987 |

Table 4 shows that for oxidation of bulk NdFeB samples at moderate temperatures activation energies were in the region of 1.1-1.2eV. This would equate to diffusion coefficients at room temperatures of around $2 \times 10^{-21} \text{cm}^2/\text{s}$. i.e. many orders of magnitude greater than the diffusion coefficient calculated for oxide growth in the present work at room temperature. Clearly for bulk NdFeB magnets at a higher temperature there are different oxide growth mechanisms and kinetics at work compared to the room temperature oxidation experiments conducted here. For powdered samples the activation energies have been reported to be around 0.5 eV, implying much more rapid oxidation rates than for bulk samples but similar to those observed here. This would be expected as powders have large surface/area ratios and oxidation will be dominated by low activation energy surface processes and defect enhanced diffusion. The rates observed in the present work are thus in keeping with defect enhanced or interstitial migration processes of oxygen.

5.4. Scoring experiments

5.4.1. 3D confocal Microscopy

It was evident from the hydrogen decrepitation experiments on the commercial rotors, which been exposed to air for prolonged periods, that surface activation of the magnets is required break through any surface oxides/contaminates prior to hydrogen processing. One possible method that was used to do this was simple scoring with a scalpel. The 3D-Confocal was used to assess the score depth using this technique. It is important to understand the score which is achieved, as this needs to be deeper than the oxide layer in order for fresh un-oxidized material to be exposed to hydrogen. It can be observed in

Table 6 that scoring numerous times increases the depth of the score, with a single score achieving a depth of 9.8 microns and scoring four times resulted in a depth of 30 microns. A Maplins N48FT Dremel tool was also used in order to create a greater level of damage. The dremel tool achieved an intermediate depth of 17.1 microns however this tool has a greater width than the scalpel blade which exposes more fresh material to hydrogen.

3D confocal image

2D optical image

2D intensity map

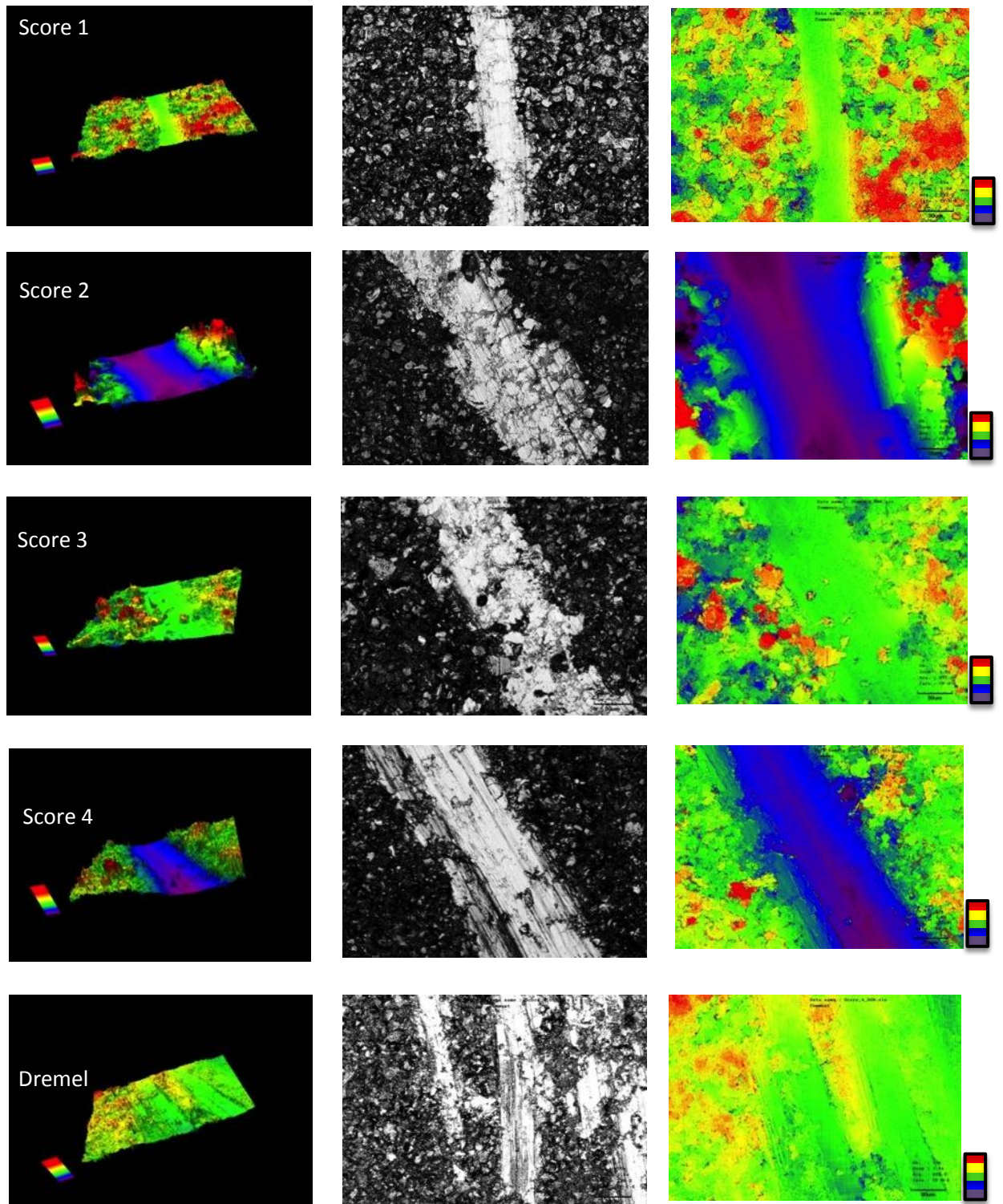


Figure 29 - Confocal Images of several score depths produced with a scalpel and a dremel tool on the surface of a NdFeB magnet.

Table 6 - Average depth of score when scored with a scalpel and imaged with a confocal microscope at x50 magnification.

| | Average Depth (μm) |
|---------|---|
| Score 1 | 9.8 |
| Score 2 | 13.9 |
| Score 3 | 15.3 |
| Score 4 | 30.3 |
| Dremel | 17.1 |

It was evident from the SEM cross sections that oxygen had penetrated the surface of the NdFeB magnets up to a depth of approximately $5\mu\text{m}$ in the triple points. Therefore scoring in this manner should easily be sufficient to break through any surface oxide. This was confirmed by the fact that scoring did result in hydrogen decrepitation on the commercial rotor. It was interesting to note that on the commercial rotors, once the magnets were scored, if the magnets were not placed into hydrogen within the first ten minutes then hydrogen would not react with the magnets, even after four hours. This was not the case for the voice coil magnets used in the coating experiments. Walton et al, 2012 has shown that voice coil magnets can be broken and then air exposed for >20 days and they would still react in hydrogen. Therefore, the oxidation rate at the grain boundaries would appear to be heavily dependant upon composition. This would also suggest that the hydrogen reaction can only initiate at the Nd-rich grain boundary phase, as it is this phase that was observed to rapidly oxidise from the SEM/confocal trials.

5.5. Assessment of Thermal and Physical Impact of Hydrogen Exposure.

5.5.1. Flat Plate Assembly

When NdFeB absorbs hydrogen, it has been shown to expand by approximately 5% [Harris, 1987] with an associated exothermic reaction. Both the physical expansion of the material and the temperature change could damage a commercial assembly by either distorting the assembly that the magnets are glued into or by demagnetising the magnets that have not been selected for removal due to the temperature rise. In order to investigate these changes a mock flat plate assembly was designed (Figure 30). The mock flat-plate assembly consisted of nine square 3cmx3cmx0.5cm NdFeB magnets mounted on a steel tray. All of the magnets apart from the central magnets were coated in order to protect them from hydrogen decrepitation. The central magnet was un-coated and was scored with a cross. Earlier experiments in this work had shown that scoring was an effective way of breaking through the oxide layer of the NdFeB magnet and ensuring that the magnet would react.

Figure 30 also displays the temperature logging hardware used in this work. This hardware was designed to be placed within the hydrogen vessel and operated using battery power. Three temperature sensors were placed upon the sample. Sensor one was placed on the resin between the central magnet and one of the outer magnets. If the sensor was positioned on the central magnet then it would have become detached once the magnet surface began to decrepitate. The second sensor was attached to one of the surrounding coated magnets. This would give an indication of the temperature increase that the surrounding magnets were exposed to when the central magnet was removed. The third sensor was positioned to measure the temperature of the steel part of the assembly. This was mounted on the underside of the base plate.

The flat plate assembly was exposed for two hours in 2b of hydrogen at room temperature. Upon removal, the assembly was photographed (Figure 31) and it was observed that the central magnet,

which had been left un-coated, had been completely decrepitated by the hydrogen (Figure 31d). The same brittle, compacted hydrided powder that was observed in the commercial assembly investigated earlier remained in the centre of the magnet. However, it was easily removed with a brush after hydrogen decrepitation.

However, upon further examination of the flat-plate assembly it was obvious that substantial damage had been caused to the base plate and the surrounding magnets. This can be observed in Figure 31 b and c. The hydrogen decrepitation test had caused considerable strain to the steel base plate causing it to bend along the line that is drawn Figure 31a. The effect of this was to cause the brittle NdFeB magnets to crack along this line, damaging the magnets and exposing fresh NdFeB magnet material to hydrogen. It appeared that the surrounding magnets then began to decrepitate and further damage was caused before the end of the experiment (Figure 31 b and c). Distortion of this flat plate assembly demonstrates that substantial force is generated during the hydrogen decrepitation process that is transmitted in all directions.

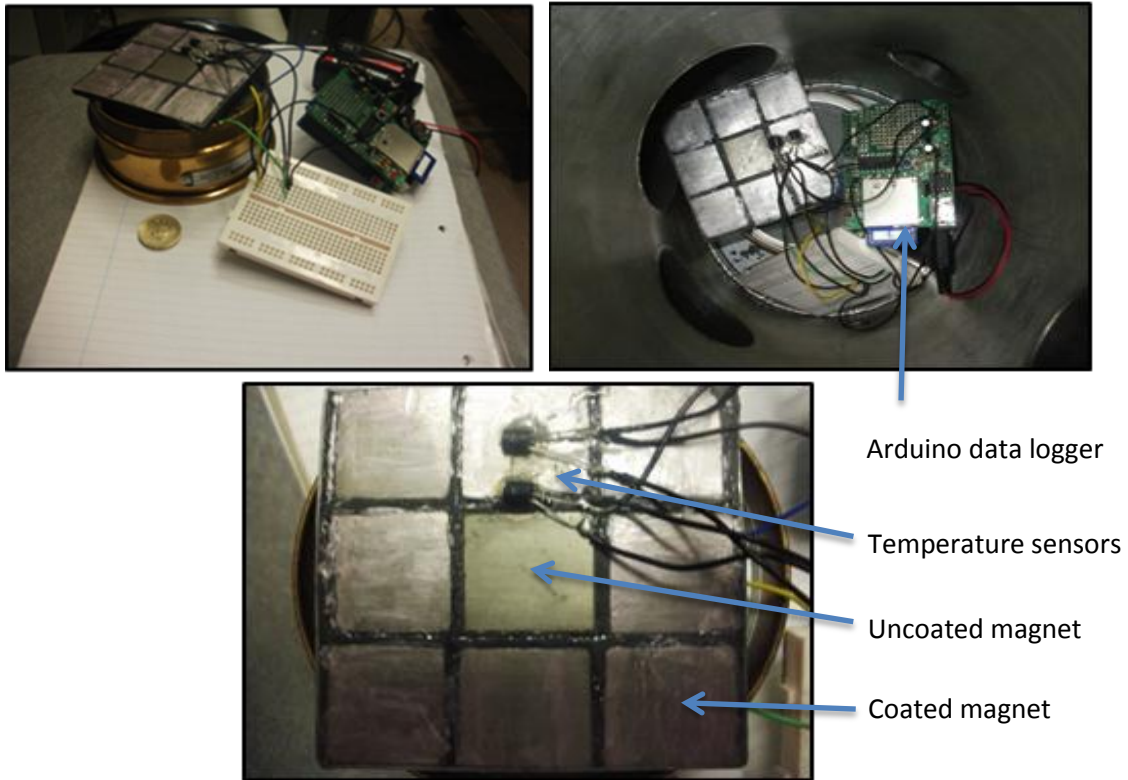


Figure 30 - Mock flate plate assembly and temperature recording apparatus.

Therefore, these results show that further work needs to be performed in order to characterize the strain that is developed when an NdFeB magnet is decrepitated. This force has been shown to be large enough in order to bend a steel base plate and damage the magnets that are contained within it. However, in a commercial assembly it is likely that the base plate would be much thicker than the steel base plate that was used in this experiment. A second consideration is that commercial assemblies are usually not flat and instead are more like the commercial assembly, which was used earlier in this work. These commercial assemblies usually have a curved surface which may cause the magnet to expand towards the surface of the magnet rather than laterally. This would have the effect of reducing the damage to the surrounding magnets as was observed in the earlier commercial assembly experiments (Figure 18).

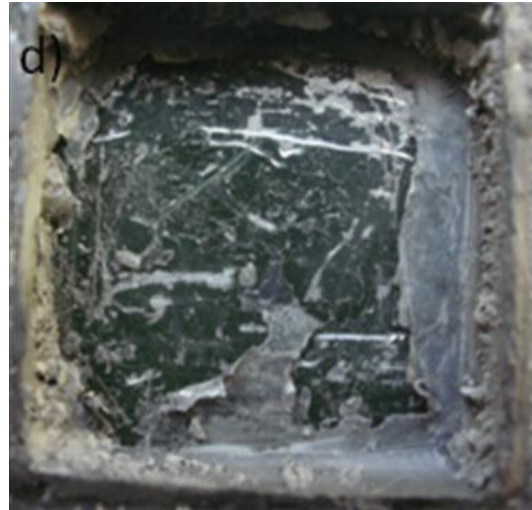
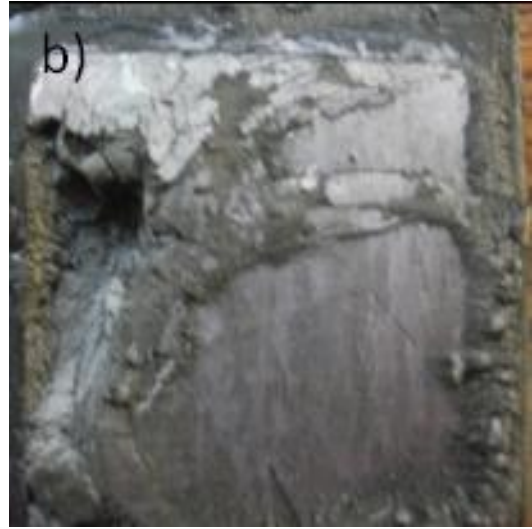


Figure 31 - Mock flate plate assembly after hydrogen decrepitation. a) Entire assembly with line drawn on to indicate bend b) damaged magnet c) damaged magnet d) Uncoated magnet removed by hydrogen decrepitation e) Side view of assembly (the thickness of the plate was 0.8 cm).

The temperature sensor, which was attached to the steel base plate, failed during the test. This was due to a problem with the analogue socket on the Arduino data logger.

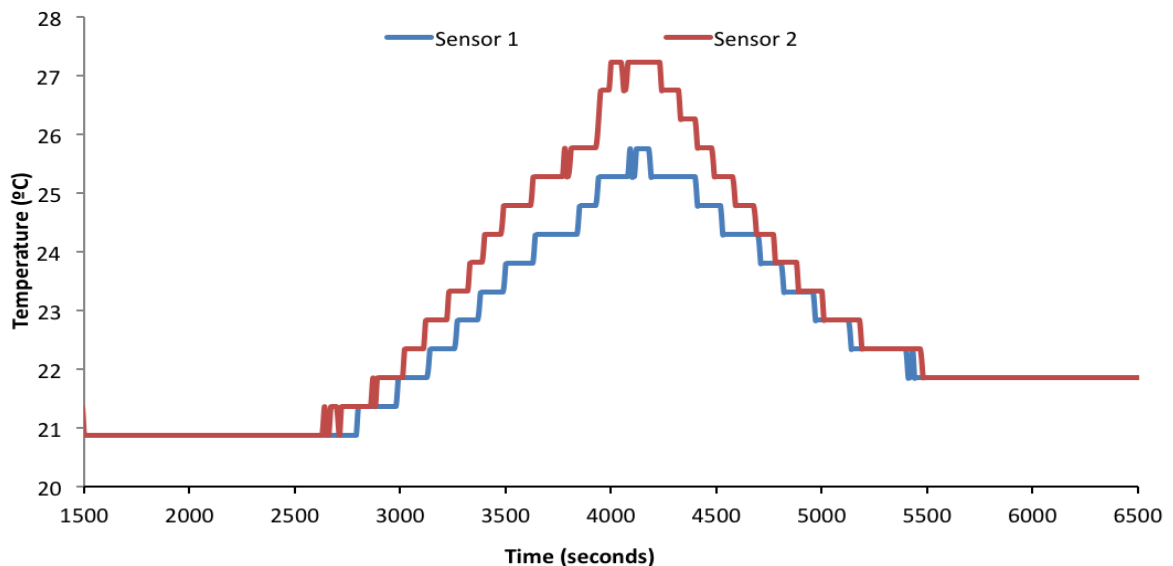


Figure 32 - Temperature data for the sensors positioned on the resin (sensor 1) and the centre of a surrounding magnet (sensor 2).

Figure 32 displays the temperature data logged from sensors 1 and 2. They show that there was an increase in temperature as the hydrogen decrepitation reaction proceeded. The plateau in the data before the peak shows the time it takes between the sample and data logger being inserted into the pressure vessel and the start of the hydrogen decrepitation reaction. There is a temperature variation of 1°C between the start and end of the reaction. This can be described by a change in the ambient temperature.

The data shows that there was a 6°C temperature increase as the hydrogen decrepitation reaction proceeded. This temperature increase is lower than was anticipated before the experiment as it has been reported that the hydrogen decrepitation of NdFeB is a highly exothermic reaction

(McGuiness, 1988). This temperature increase would not be large enough to have any significant impact on the magnetic properties of the other magnets in the assembly. This data is important as it was thought before the experiment that the temperature that was developed during the hydrogen decrepitation reaction might have been a large barrier to the use of hydrogen for removing single magnets from an NdFeB assembly. However there may be a larger temperature increase when there is more NdFeB magnet material as observed in some commercial assemblies. However there will also be a larger steel base plate, which will act as a heat sink which will conduct the heat away from the magnets.

5.5.2. MagScan

A MagScan was used to assess the magnetic field strength developed from the mock assembly at different positions. Figure 33 and Figure 34 shows the Magscan data for the flat plate assembly before and after decrepitation. It was observed that there have been significant changes in the magnetic field patterns across the assembly. The Magscan experiments were originally conducted as a way of visualizing any magnetic deterioration due to thermal degradation. However, it has become apparent that the temperature changes observed would not be sufficient to have any impact.

The dramatic changes observed are a result of the distortion of the assembly, resulting in cracking of the magnets/coating and then subsequent decrepitation of the magnets. This data demonstrates that the magnets that are cracked produce a reduced magnetic field that shows that the damage done to the magnets by cracking and subsequent hydrogen decrepitation has a dramatic effect on the magnetic properties of the magnet.

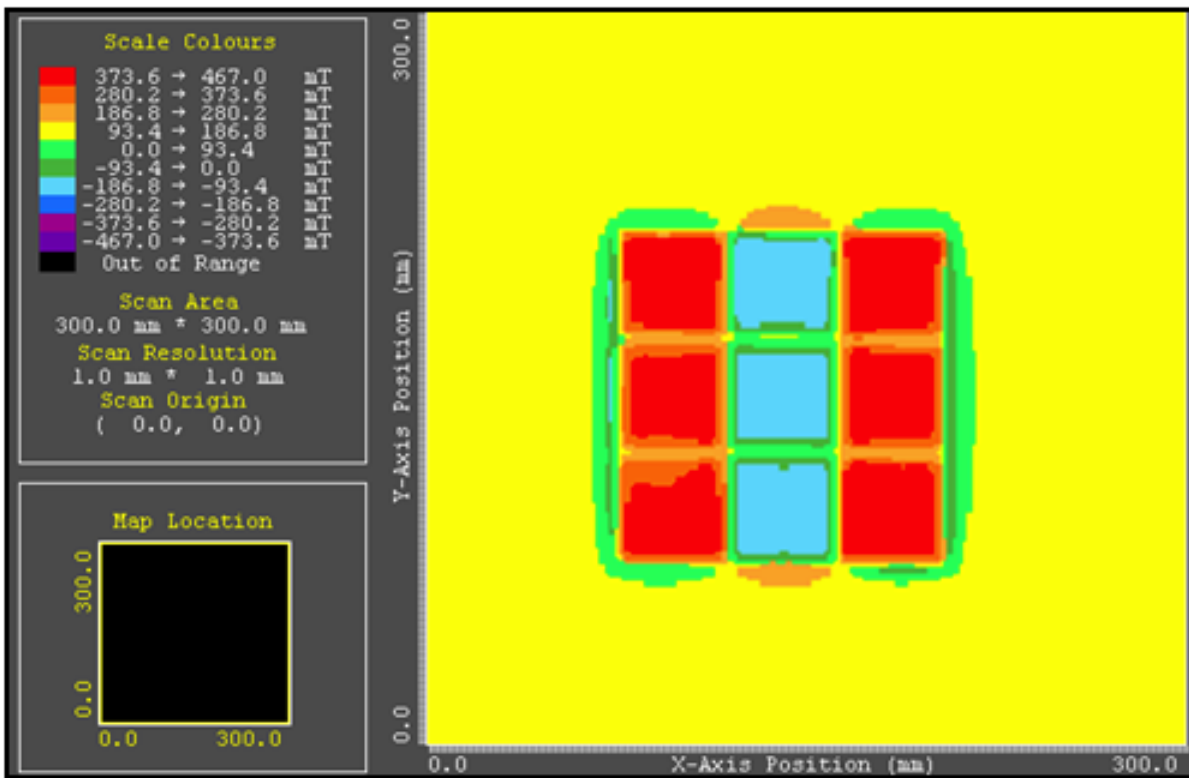


Figure 33 - MagScan data prior to hydrogen decrepitation.

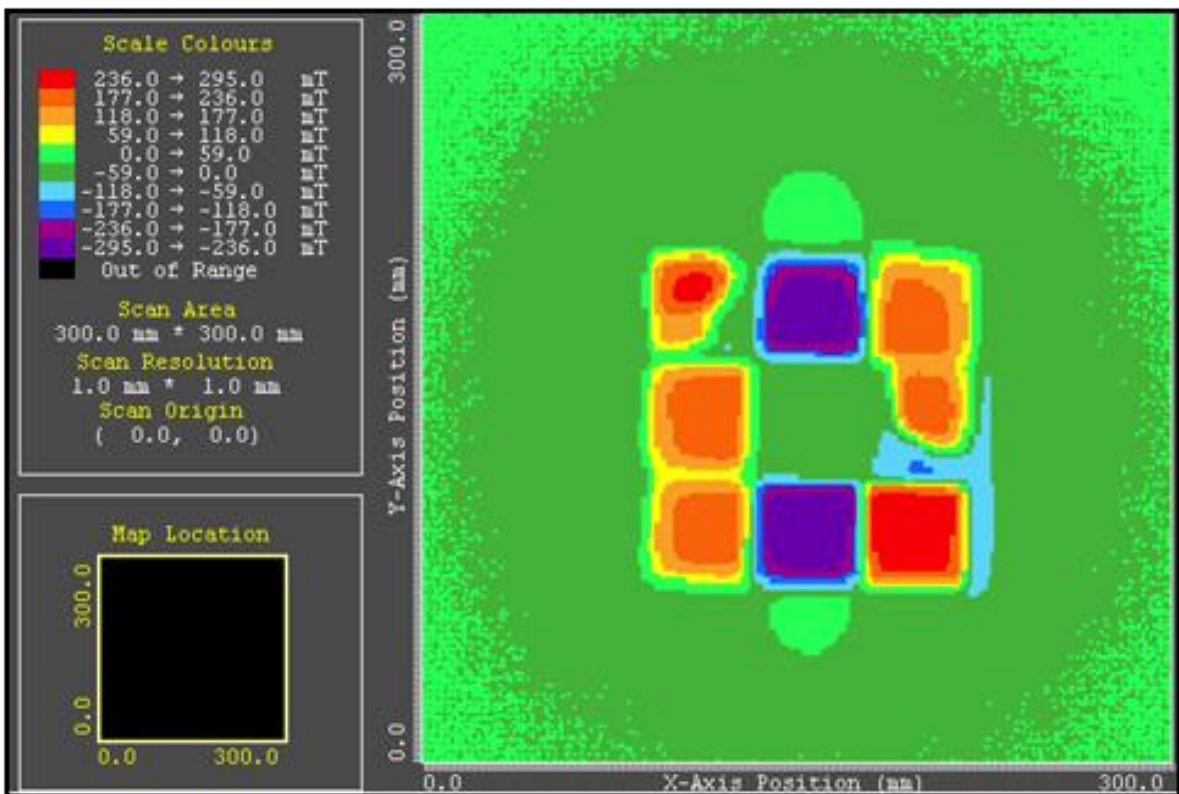


Figure 34 - MagScan data for post decrepitation.

5.6. Encapsulation of NdFeB magnets

Further to the flate plate assemblies NdFeB magnets were cut into cylinders and encapsulated Cu sleeves to investigate the impact of confinement of the material during decrepitation. This created a simpler system with fewer materials and therefore fewer variables. The magnets were voice coil assembly magnets which were cut into cylinders with a diameter of 4mm (

Figure 16). The c-axis of the magnet was pointing upwards with the flat surfaces of the NdFeB magnet being free. The magnet assembly was imaged using the tiling feature on the confocal microscope and accurate measurements were taken of the magnet and the Cu tube using a micrometer. The magnet was then exposed to hydrogen and the strain produced was characterised by the change in shape of the assembly across its width.

The samples were encapsulated and exposed to hydrogen at 2 bars for 2 hours. Samples were first encapsulated in a 1mm thick Cu tube; however, no evidence of lateral expansion could be observed. Therefore, thinner walled Cu was subsequently utilized with a wall thickness of 0.4mm. The magnets were shown to expand out of the free surface of the Cu sleeve and the Cu sleeve was shown to expand laterally. Interestingly the NdFeB magnets did not break into a hydrided powder during H₂ exposure. Significant differences in the level of expansion were observed between different samples (Table 7).

After hydrogen exposure it was possible to run a spatula across the magnet surface without

powder pull out and it was possible to remove the NdFeB from the Cu sleeves without the material further breaking down.

A non-encapsulated NdFeB magnet, which was cut out by spark erosion machining, was also exposed to hydrogen at 2 bars for 2 hours. This un-encapsulated sample did break down into a hydrided powder as usual.

Further testing was carried out at hydrogen pressures of 8 bar to make sure that the encapsulated samples had hydrided. In these experiments the samples were ground with p400 grinding paper in order to completely remove the oxide layer and also to provide a greater surface area for hydrogen decrepitation to initiate. The sample was exposed to hydrogen for 5 hours. At the end of this experiment, the magnets were imaged and measured. The sample still did not show signs of breaking into a powder at higher pressures.

The magnets could not be magnetised after hydrogen exposure which indicated that the matrix phase had reacted with hydrogen.

Using the dimensions that were obtained by using confocal microscopy, the strain on the Cu tube can be found using the formula:

$$\varepsilon = \frac{dl}{l_0} \quad \text{Equation 6}$$

Where: ε =strain; dl = change in length (m); l_0 = initial length (m).

The strain can then be used along with the Young's modulus of the Cu tube in order to find the stress that the Cu tube was placed under when the NdFeB magnet decrepitated, using the formula.

$$\sigma = \epsilon x E$$

Equation 7

Where: σ = stress (Pa); ϵ =strain; E = Young's Modulus (Pa).

To work out the energy per unit volume, the equation below is used:

$$\text{Energy per unit volume} = 0.5\sigma x \epsilon$$

Equation 8

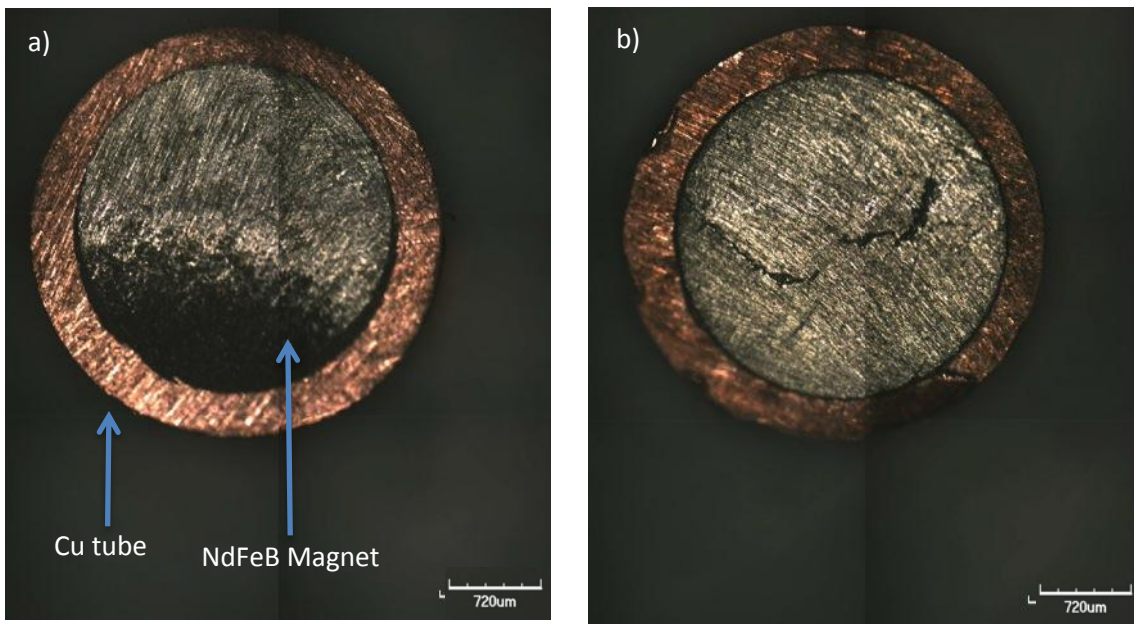


Figure 35 - Tiled optical image of an encapsulated NdFeB sample before (a) and after (b) hydrogen exposure.

Table 7 - Diameter measurements for the sample before and after exposure to hydrogen.

| | Cu Diameter Pre HD(mm) | Cu Diameter Post HD (mm) | Change in diameter (mm) | Stress (MPa) | Energy per unit volume (J/m ³) |
|----------|---------------------------|-----------------------------|----------------------------|--------------|---|
| Sample 1 | 3.861 | 3.927 | 0.066 | 23 | 2357 |
| Sample 2 | 3.869 | 4.02 | 0.161 | 52 | 12364 |

Large variations in the diameter of the Cu can be observed in Table 7 for the sample after HD treatment. This could be due to a number of reasons including uneven spacing between the magnet and the Cu sleeve, inaccuracy of the confocal tiling technique and variations in the surface roughness of the magnet. Therefore the values generated for strain, stress and energy are only indicative values. However, as far as the author is aware this is the first time any data has been generated on the level of stress caused by the HD process on encapsulated NdFeB.

This is a preliminary experiment and more testing needs to be performed to improve the accuracy of this technique. This experiment has allowed for an estimation of the forces that are generated during the hydrogen decrepitation reaction which can provide useful information for further experimentation. Typically this situation would be considered using equations which relate to hoop stress rather than the change in length of the copper. However, the equations for hoop stress require data for not only the wall thickness and the length of the cylinder but the internal pressure acting on the cylinder, this is shown in equation 9.

$$\sigma_0 = \frac{F}{tl} \quad \text{Equation 9}$$

Where: F is the force extended circumferentially on the cylinder wall; t is the radial thickness of the cylinder; l is the axial length of the cylinder. Therefore, equation 7 was used in order to provide a rough estimate of the forces developed during hydrogen decrepitation.

6. Conclusions

Several coatings were tested as barrier coatings against hydrogen decrepitation. Nail varnish and Gestetner lithographic correction fluid have both been shown to act as protective layers against hydrogen that would allow sufficient time to remove other magnets from an assembly. The coatings are likely to only have a slow diffusion rate for hydrogen. Therefore, if prolonged periods of hydrogen exposure were endured the magnets would be likely to react. It is likely that a wide

variety of different coating materials could play a similar role.

This work showed that either some or all of the NdFeB magnets could be removed successfully from a commercial assembly. When the magnets were removed from the smart car rotor the steel rotor was found to be undamaged. The decrepitated magnetic material was shown to be demagnetised and fell to the bottom of the reaction vessel as a powder. This powder could then be collected and recycled using the same methods reported by Zakotnik (2009).

Investigations on removing a single magnet from a mock flat plate assembly demonstrated that large amounts of sub – surface strain are developed. This was displayed in the mock flat plate assembly experiment as there was a large distortion of the steel base plate which caused two of the surrounding magnets to crack and begin to hydrogen decrepitate. However most large scale magnet applications are likely to have a much more substantial base plate/rotor to cope with the magnetic forces which are generated. Therefore, the impact of the strain developed during decrepitation may not manifest itself as a dimensional change in the base structure. When decrepitating magnets from the Smart Car rotor, no change in size could be observed and none of the other magnets in the assembly were damaged.

Temperature sensors were attached to the assembly in order to characterise the temperature rise which is generated by the hydrogen decrepitation reaction and to assess whether the heat generated would be high enough to have a demagnetising effect on the surrounding magnets. It was shown that it is very unlikely that hydrogen decrepitation of individual magnets from an assembly that enough heat would generate enough heat to permanently damage the magnetic field in the surrounding magnets. Aktar (2010) showed that this would need to be greater than 80°C in order to permanently effect the NdFeB magnets. On a commercial assembly where there will be larger amounts of magnetic material and therefore the possibility of generating larger amounts of heat is increased. However, the substrate/rotor is likely to provide a very large heat

sink that will reduce the temperature rise observed in neighbouring magnets.

The Flat plate assembly was imaged using a Magscan before and after the hydrogen decrepitation reaction in order to characterise any changes in the magnetic field which is generated by the assembly. The Magscan data showed that substantial changes in the magnetic field pattern across the assembly were observed. This was due to the distortion of the plate and subsequent decrepitation of the magnets rather than being as a result of temperature fluctuations

It has been shown that scoring of the NdFeB magnets to expose fresh material plays an important role in initiating the HD process. The magnets mounted on commercial rotors needed to be scored in order for decrepitation to take place. However, the voice coil magnets used for the coating experiments, required no such scoring. This could be due to two reasons. Firstly, the magnets have different compositions and secondly the magnets have different levels of surface oxide. The voice coil magnets were coated in Ni (which was stripped off prior to the hd process). It is therefore necessary to characterise the oxide layer which forms on the surface of the NdFeB magnets in order to gain a greater understanding of the initiation of the hydrogen decrepitation reaction.

It would therefore appear that the HD process must initiate at these Nd-rich regions as in some cases after 30 minutes of air exposure after scoring the HD process would not work. This confirms previous work by Harris et al who postulated that the HD process must initiate at grain boundaries and triple points.

This work has demonstrated that the 3D confocal microscope is a very powerful tool for observing metal-gas interactions. In future work a pressure cell will be fitted to the microscope which can be filled with hydrogen. It should then be possible to directly observe the HD process initiating at triple points.

A combination of SEM equipped with WDS, raman spectroscopy and 3D confocal microscopy has

clearly shown that the Nd-rich triple points oxidise preferentially compared to the matrix phase on bulk sintered NdFeB magnets in atmospheric conditions at room temperature. This is not the case for higher temperature oxidation [Edgley, 1997] where a planar oxidation front has been observed passing through both the grain boundaries/triple points and matrix grains. The diffusion coefficient calculated from the oxide growth data ($3 \times 10^{-13} \text{ cm}^2/\text{sec}$) further suggested a grain boundary type mechanism for oxide growth. This is the first time that such a dominant grain boundary mechanism has been demonstrated for bulk sintered magnets under these conditions.

It has been observed in this work that this grain boundary oxidation is more rapid than has been reported previously by Jacobson et al [1987], where the weight gain of a sample was measured over a time period of weeks rather than minutes. The implications of these findings is that there is a very short time period between exposure of some samples to oxygen before they will no longer be affected by hydrogen decrepitation without first breaking the NdFeB alloy to expose clean material. To achieve reproducible hydrogen decrepitation of scrap magnet material that has been exposed to atmospheric conditions it will be necessary to add a further surface pre- processing step.

In this project scoring with a scalpel was used to initiate the hydrogen decrepitation reaction. Scoring experiments showed that the score depth of an NdFeB magnet scored with a scalpel is around $10 \mu\text{m}$ and this can be increased by scoring the sample a number of times. A dremel tool was also tested and this proved to be an effective scoring method as it scored to a depth of $17 \mu\text{m}$ in a wider area than could be achieved with a scalpel exposing more un- oxidised material to hydrogen. In the SEM equipped with WDS investigations it was shown that the oxide layer was approximately $3 \mu\text{m}$ thick. Therefore scoring with a scalpel should be of sufficient depth to break through the oxide layer and initiate hydrogen decrepitation. This was shown to be the case.

In an attempt to understand the impact of encapsulation of NdFeB magnets on the HD process

several sintered magnets were embedded in copper sleeves. When the sleeved assemblies were processed in hydrogen surprisingly the NdFeB magnets stayed intact even after removal from the sleeve. This is the first time that such a phenomenon has been observed. This has implications on the use of hydrogen as a tool for separation of magnets from assemblies, as if they are heavily embedded the HD process will not reduce them to a powder which can be stripped from the device. This was only a preliminary study and further work is required to understand the underlying mechanisms.

The work outlined in this project was the first attempt to investigate the use of hydrogen decrepitation to remove magnets from large commercial assemblies and to determine the impact of oxidation on the HD process. The results have raised a large number of questions and possible future work including:

- Investigate the oxidation rate of a larger range of NdFeB sintered magnet compositions.
- In-situ 3D confocal microscopy of the HD process.
- Further investigation of the hydrogen absorption mechanism in encapsulated NdFeB magnets including gravimetric studies and X-ray diffraction.

7. References

Akhtar, A. Haider, Z. Ahmad, M. Farooqu, 2010, Development of NdFeB Magnet through Hydrogen Decrepitation, Key Engineering Materials, Vol. 442, pp. 263-267.

Bai, G, Gao, R, Sun, Y, Han, G, Wang, B, 2007, Study of high-coercivity sintered NdFeB magnets, Journal of Magnetism and Magnetic Materials, vol. 308, pp. 20-23.

R. Blank, E. Alder, 9th International Workshop on Rare Earth Magnets and Their Applications[1987].

Boller, H, Oesterreicher, H, 1984, On the structure of Nd₂Fe₁₄B, Journal of Less Common Metals, vol. 103, pp. 5-7.

Chinnasamy, C. Jasinski, M, M. Li, W. Walmer, M. Dent, p. Hadjipanayis, G. Lui, J, 2012, Mn-B Powders with High Coercivity and Magnetization at Room Temperature, The 22nd Workshop on REPM.

Coey, J.M.D, 1995, Rare-earth magnets, Endeavour, Vol. 19, pp. 146-151.

Croat, J. J, Herbst, J. F, Lee, R. W, Pinkerton, F. E, 1984, Pr-Fe and Nd-Fe-based materials: A new class of high-performance permanent magnets, Journal of Applied Physics, vol. 55, pp. 2078-2082.

Cullity, B. Graham, C. 2009. Introduction to Magnetic Materials. Second Edition. Wiley: New Jersey.

Edgley, D, Breton, J, Steyaert, S, Ahmed, F, Harris, I, Teiller, J, 1997, Characterisation of high temperature oxidation of Nd-Fe-B magnets, Journal of Magnetism and Magnetic Materials, vol. 173, pp. 29-42.

D.S. Edgley, J.M. LeBreton, D. Lemarchard, I.R. Harris and J. Teillet: Journal of Magnetism and magnetic materials[1993], 128, pL1-L7.

Fidler, J, 1987, On the role of the ND-rich phases in sintered ND-FE-B magnets, IEEE Transactions on Magnetism, vol. 23, pp. 2106-2108.

Givord, D, Li, H, Moreau, J, 1984, Relationships Between Crystal Structure and Magnetic Properties in Nd₂Fe₁₄B, Solid State Communications, vol. 50, pp. 497-499.

Gutfleisch, O. Willard, M. Bruck, E. Chen, C. Sankar, S. Liu, J. 2011. Magnetic Materials and Devices for the 21st Century: Stronger, Lighter, and More Energy Efficient. Advanced Materials. Vol: 23 pp:821-842.

Harris. I.R. 1987, The Potential of Hydrogen in Permanent Magnet Production, Journal of the Less-common Metals, vol. 131, pp. 245 – 262.

Herbst, J, F, Croat, J, J, Yelon, W, B, 1985, Structural and magnetic properties of Nd₂Fe₁₄B, Journal of Applied Physics, vol 57, pp. 4086-4090.

Herbst, J,F, Croat, J, Pinkerton, F, Yelon, W, 1984, Relationships Between Crystal Structure and Magnetic Properties in Nd₂Fe₁₄B, Physical Review B, Vol. 29.

Higgins, B, Oesterreicher, H, 1987, Properties and Stability of Nd₂Fe₁₄B Particles, IEEE Transactions on Magnetism, vol. 23, pp. 92-94.

Jacobson, J, Kim, A, 1987, Oxidation Behaviour of NdFeB magnets, Journal of Applied Physics, vol. 61, pp. 3763- 3766.

Kaneko, Y, Kuniyoshi, F, Ishigaki, N, 2006, Proven technologies on high-performance Nd–Fe–B sintered magnets, Journal of Alloys and Compounds, vol. 408, pp. 1344-1349.

Kim, A, Camp,F, 1995, Effect of Minor Grain Boundary Additives on the Magnetic Properties of NdFeB Magnets, IEEE Transactions on Magnetism, vol.31, pp. 3620-3623.

Kim, A, Camp, F, 1996, High Performance NdFeB Magnets, Journal of Applied Physics, vol. 79, pp. 5035-5040.

Knoch, K, Schneider, G, Fidler, J, Henig, E, Kronmuller, H, 1989, Al- Doped NdFeB permanent magnets: Wetting and microstructural investigations, IEEE Transactions on Magnetism, vol. 25, pp. 3426-3429.

J.M. LeBreton, J.Teillet, P.J. Mc Guinness, D.S. Edgley and I.R. Harris: IEEE Trans. Magn. [1992] ,28, p2157.

D. Lemarchand, J. Delamare, P. Vigier. J. Appl. Phys [1992] Vol. 72, p. 1996.

Li, J, Gao, S, Li, M, Wang, Y, Tu, M, 2006, Effect of process on the magnetic properties of bonded NdFeB magnet, Journal of Magnetism and Magnetic Materials, vol. 299, pp. 195-204.

Li, Y, Evans, H, Harris, I, Jones, P, 2002, The Oxidation of NdFeB Magnets, Oxidation of Metals, vol. 59, pp. 167 – 183.

Lui, W, Liang, Y, Bounds, C, 1992, Effects of Nb Addition and/or Casting Method on the Amount of Precipitated Fe in NdFeB Alloys, IEEE Transactions on Magnetism, vol. 28, pp. 2154-2157.

McGuinness, P, 1989, The Study of NdFeB hydrides and their application to the production of permanent magnets, Thesis submitted for the Degree of Doctor of Philosophy, The University of Birmingham.

P.Mele , C.Artini, A.Ubaldini, G.A.Costa, M.M.Carnasciali, R.Masini, Journal of Physics and Chemistry of Solids [2009] Vol. 70 p276.

Ohring, 1995, Engineering Materials Science, Chester: Academic Press.

Z. Osawa, M. Higuchi, S. Hinohara, J. Mater. Sci. 1992. Vol. 27 p5445.

Pandian, S, Chandrasekaran, V, 2002, Effect of Al, Cu, Ga, and Nb additions on the magnetic properties and microstructural features of sintered NdFeB, *Journal of Applied Physics*, vol. 92, pp. 6082-6087.

Sagawa, M, Fujimura, S, Togawa, N, Yamamoto, H, Matsuura, Y, 1984, New material for permanent magnets on a base of Nd and Fe, *Journal of Applied Physics*, vol. 55, pp. 2083-2087.

Shoemaker, C, Shoemaker, D, Fruchart, 1984, The structure of a new magnetic phase related to the sigma phase: iron neodymium boride Nd₂Fe₁₄B, *Acta Crystallographica*, vol. 40, pp. 1665-1668.

Skulj, H. E. Evans, I. R. Harris, 2008, Oxidation of NdFeB-type magnets modified with additions of Co, Dy, Zr and V, *Journal of Materials Science*, vol. 43, pp. 1324–1333.

Song, X, Lu, N, Seyring, M, Rettenmayr, M, Xu, W, Zhang, Z, Zhang, J, 2009, Abnormal crystal structure stability of nanocrystalline Sm₂Co₁₇ permanent magnet, *Applied Physics Letters*, vol. 94, Issue 2 pp. 023102 - 023102-3.

M. Stewart. B Roebuck. M.G. Gee. *J. Mater. Sci* [1991] Vol. 26. p1401.

Strnat, K, Hoffer, G, Olson, J, Ostertag, W, Becker, J, 1967, A Family of New Cobalt-Base Permanent Magnet Materials, *Journal of Applied Physics*, vol. 38, pp. 1001-1002.

Sun, A, Wu, S, Xu, W, Wang, J, Zhang, Q, Zhai, F, Volinsky, A, 2012, Nd₂Fe₁₇ nanograins effect on the coercivity of HDDR NdFeB magnets with low boron content, *International Journal of Minerals, Metallurgy and Materials*, vol: 19, p: 236.

Tenaud, P, Lemaire, H, Vial, F, 1991, Recent improvements in NdFeB sintered magnets, *Journal of Magnetism and Magnetic Materials*, vol.101, pp. 328-332.

K. N. Tu, J. W. Mayer, L. C. Feldman, 1992, *Electronic Thin Film Science*, Macmillan Publishing Company, New York.

A. Walton, A. Willams, 2011, Rare Earth Recovery, *Materials World*, August 2011.

A. Walton, H. Yi, V. Mann, A. Bevan, J. Speight, I.R. Harris, A. Williams, 2012, The Use of Hydrogen to Separate and Recycle NdFeB Magnets from Electronic Waste.

J. Wang,, G. Xiao, X. Yizhuang, Z. Yong, X. Boqing, C. Shun, D. Wang, X. Duanfu, Journal of Crystal Growth [2006] Vol.268. p. 78.

Williams, A, 1994, Thesis, University of Birmingham.

H.Y. Wong, A.G. Clegg, G. Hinton, Oxidation and Corrosion Behaviour of Nd-Fe-B Magnets[1990].

Yu, L, Wen, Y, Yan, M, 2004, Effects of Dy and Nb on the magnetic properties and corrosion resistance of sintered NdFeB, Journal of Magnetism and Magnetic Materials, Vol .283, PP. 353-356.

Zakotnik, M, Harris, I, Williams, A, 2009, Multiple recycling of NdFeB-type sintered magnets, Journal of Alloys and Compounds, Vol. 469, pp. 314–321.

Zakotnik, M, Harris, I, Williams, A, 2008, Possible methods of recycling NdFeB-type sintered magnets using the HD/degassing process, Journal of Alloys and Compounds, vol. 450, pp. 525-531.

Zakotnik, M, 2004, The Recycling of NdFeB Sintered Magnets Using the HD Process. Thesis, University of Birmingham.

http://en.wikipedia.org/wiki/File:UK_windfarm_growth.PNG> (viewed on 03/08/2011)

<http://www.magnets.bham.ac.uk/magneticmaterials/historupdatey.shtml> <viewed on the 29/06/2011>